

## Copper and gold cyclic (alkyl)(amino)carbene complexes with sub-microsecond photoemissions: Structure and substituent effects on redox and luminescence properties

Alexander S. Romanov,<sup>\*[a]</sup> Ciaran R. Becker,<sup>[a]</sup> Charlotte E. James,<sup>[a]</sup> Dawei Di,<sup>[b]</sup> Dan Credgington,<sup>\*[b]</sup> Mikko Linnolahti<sup>\*[c]</sup> and Manfred Bochmann<sup>\*[a]</sup>

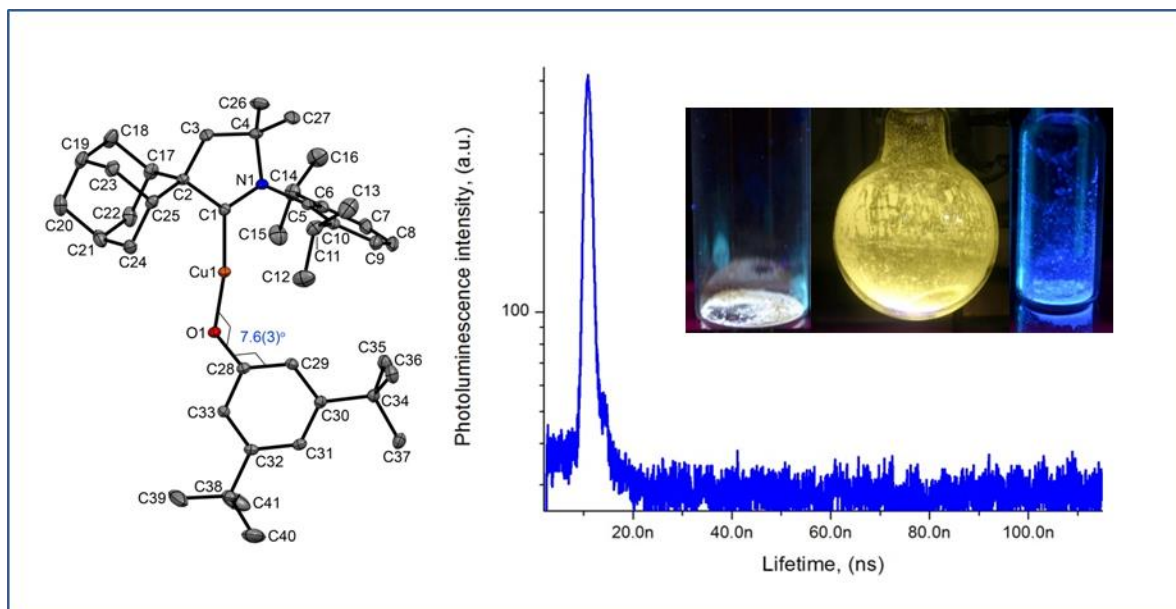
<sup>[a]</sup> Dr. A. S. Romanov, C. R. Becker, C. E. James, Prof. M. Bochmann, School of Chemistry, University of East Anglia, Earlham Road, Norwich, NR4 7TJ, UK;

<sup>[b]</sup> Dr. D. Di, Dr. D. Credgington, Department of Physics, Cavendish Laboratory, Cambridge University, Cambridge CB3 0HF, UK

<sup>[c]</sup> Prof. M. Linnolahti, Department of Chemistry, University of Eastern Finland, Joensuu Campus, FI-80101 Joensuu, Finland

**Keywords:** Carbene ligands; photoluminescence; gold complex; copper complex; structure determination; fluorescence; electrochemistry

### Table of Contents Entry



Copper and gold complexes stabilized by cyclic (alkyl)(amino)carbene ligands ( $^R\text{L}$ )MX, where X = halide, pseudo-halide, amide or aryloxy represent a large class of photoluminescent materials, with emission lifetimes ranging from nanosecond to microsecond regimes.

**ABSTRACT:**

Copper and gold halide and pseudo-halide complexes stabilized by methyl-, ethyl- and adamantyl-substituted cyclic (alkyl)(amino)carbene (CAAC) ligands are mostly linear monomers in the solid state, without aurophilic Au...Au interactions. (<sup>Ei2</sup>L)CuCl shows the highest photoluminescence quantum yield (PLQY) in the series, 70%. The photoemissions of <sup>Me2</sup>L and <sup>Ei2</sup>L copper halide complexes show S<sub>1</sub> → S<sub>0</sub> fluorescence on the ns time scale, in agreement with theory, as well as a minor long-lived emission. Monomeric (<sup>Me2</sup>L)CuNCS is a white emitter, while dimeric [(<sup>Ei2</sup>L)Cu(μ-NCS)]<sub>2</sub> shows intense yellow emission with a PLQY of 49%. The reaction of (<sup>Ad</sup>L)MCl (M = Cu or Au) with phenols ArOH (Ar = Ph, 2,6-F<sub>2</sub>C<sub>6</sub>H<sub>3</sub>, 2,6-Me<sub>2</sub>C<sub>6</sub>H<sub>3</sub>, 3,5-Bu'<sub>2</sub>C<sub>6</sub>H<sub>3</sub>, 2-Bu'-5-MeC<sub>6</sub>H<sub>3</sub>, 2-pyridyl), thiophenol, or aromatic amines H<sub>2</sub>NAr' (Ar' = Ph, 3,5-(CF<sub>3</sub>)<sub>2</sub>C<sub>6</sub>H<sub>3</sub>, C<sub>6</sub>F<sub>5</sub>, 2-py) afforded the corresponding phenolato, thiophenolato and amido complexes. Whereas the emission wavelengths are only marginally affected by the ring substitution pattern, the PL intensities respond sensitively to the presence of substituents in *ortho* or *meta* position. In gold aryloxides PL is controlled by steric factors, with strong luminescence in compounds with Au-O-C-C torsion angles <50°. Calculations confirm the dependence of oscillator strength on the torsion angle, as well as the inter-ligand charge transfer nature of the emission. The HOMO/LUMO energy levels were estimated based on first reduction and oxidation potentials.

**Introduction**

As we have shown recently, halide complexes of copper and gold form linear mononuclear complexes with cyclic (alkyl)(amino)carbene (CAAC) ligands which have interesting photoluminescence (PL) properties, with the copper(I) chloride adducts reaching a photoluminescence quantum yield (PLQY) in the solid state of up to 96%.<sup>[1]</sup> This high PL efficiency was due to the very fast rate of fluorescence (>10<sup>9</sup> s<sup>-1</sup>) and the low geometric distortion in the excited state, which minimises non-emissive pathways.

Photoluminescent coinage metal complexes stabilised by unsaturated imidazolylidene-type *N*-heterocyclic carbenes (NHCs) are of course well-known.<sup>[2]</sup> The first example of a photoemissive copper complex in this category was a binuclear dication [Cu<sub>2</sub>{(NHC)<sup>^(</sup>(NHC)}<sub>2</sub>]<sup>2+</sup>, which shows blue-green phosphorescence.<sup>[3]</sup> Similar photoemissions were found for a range of ionic or zwitterionic heterobinuclear copper-gold complexes, for example [Au{(NHC)<sup>^(</sup>(heterocycle)}<sub>2</sub>CuL<sub>2</sub>]<sup>2+</sup> and larger aggregates, with carbene-coordinated Au and N-bonded three- or four-coordinate Cu ions (heterocycle = pyridine or quinolone); in these cases the ligands themselves are also luminescent.<sup>[4]</sup> Three-coordinate Cu(I) carbene complexes [(NHC)Cu(N<sup>^</sup>N)]<sup>n+</sup> (n = 0, 1, where N<sup>^</sup>N is either a neutral or anionic pyridine-based donor) were found to be strongly emissive.<sup>[5]</sup> In contrast, simple copper halide adducts of imidazolylidene-type carbenes (NHC)CuX are non-emissive.

Photoluminescent gold(I) NHC complexes may be neutral, as in (NHC)AuX, or cationic, [Au(NHC)<sub>2</sub>]<sup>+</sup>. Early examples are the benzimidazolylidene derivatives reported by Lin and co-workers, (benzimid)AuX (X = halide, SPh, C<sub>2</sub>Ph, carbazolate), which show blue to yellow phosphorescence.<sup>[6]</sup> More recently Nolan et al. described a related series of NHC gold anilide complexes with a similar photoluminescence range but low intensity in most cases.<sup>[7]</sup> By contrast, Gimeno et al. reported three-coordinate NHC gold(I) complexes which gave high solid-state PLQYs; the co-ligand in this case was a bidentate bis(phosphino)carboranyl anion.<sup>[8]</sup>

The photoemissive <sup>Ad</sup>CAAC complexes we reported earlier<sup>[11]</sup> differ from these NHC compounds by their efficient prompt fluorescence on the sub-nanosecond time scale, rather than phosphorescence, most probably enhanced by the known  $\pi$ -acceptor properties of CAAC ligands which exceeds that of NHCs.<sup>[9]</sup> In an effort to establish a structure-property relationships in photoemissive copper and gold CAAC compounds, we have explored a number of different types of CAAC ligands of varying degrees of steric hindrance, <sup>Me2</sup>L, <sup>Et2</sup>L and <sup>Ad</sup>L (Chart I), and report here the syntheses, structures and properties of a range of halide, pseudo-halide, aryloxyde and amide complexes in terms of their suitability for the fabrication of light-emitting devices.

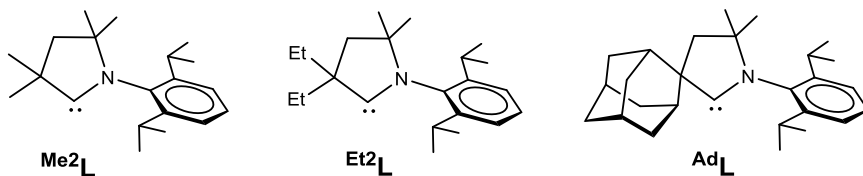


Chart I

## Results and Discussion

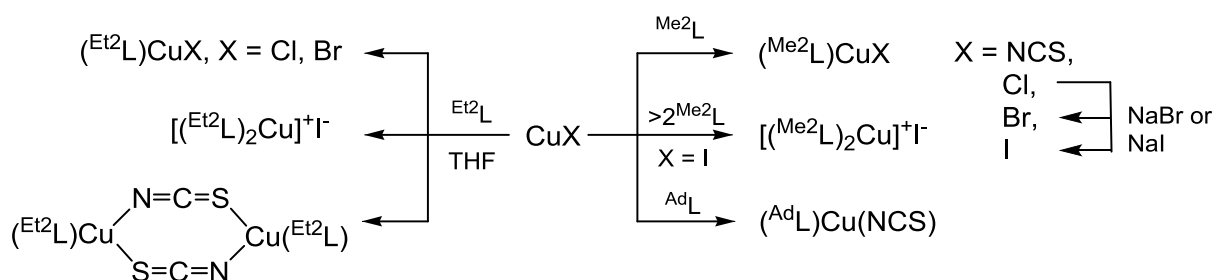
### Synthesis and structure

*Copper halide and pseudo-halide complexes.* Copper(I) halide and pseudo-halide complexes with ligands <sup>Me2</sup>L, <sup>Et2</sup>L and <sup>Ad</sup>L were prepared as shown in Scheme 1, by combining a solution of the respective CAAC ligands with copper salts in THF, following procedures previously established for gold halide complexes.<sup>[10,11]</sup> While this work was in progress, the syntheses of (<sup>Me2</sup>L)CuCl and (<sup>Et2</sup>L)CuCl were reported independently,<sup>[12]</sup> the compounds are included in Scheme 1 for completeness. While the reaction of <sup>Me2</sup>L with CuCl is essentially quantitative, the yields of (<sup>Me2</sup>L)CuX (X = Br, I) are moderate due to the formation of insoluble by-products. However, high yields of the bromo and iodo complexes can be obtained by metathesis of (<sup>Me2</sup>L)CuCl with NaBr or NaI, respectively. An excess of <sup>Me2</sup>L affords the 2:1 complex [(<sup>Me2</sup>L)<sub>2</sub>Cu]I. The halide complexes show good solubility in polar non-protic solvents like

dichloromethane, THF, MeCN, DMF or acetone and are moderately soluble in toluene or ethanol but insoluble in hexane.

A very recent paper claimed that the 2:1 compounds  $[(^{\text{Me}2}\text{L})_2\text{Cu}]X$  are unstable for  $X = \text{Cl}, \text{Br}$  or  $\text{I}$  and could not be isolated.<sup>[13]</sup> In our hands,  $[(^{\text{Me}2}\text{L})_2\text{Cu}]\text{I}$  proved stable to air and moisture for extended periods of time and was isolated in 97% yield.

The neutral CAAC copper halide complexes are thermally very stable and can be sublimed at 200 °C / 0.3 mm Hg without decomposition. They are also stable in air for several weeks and indefinitely stable under argon. Thermogravimetric and differential scanning calorimetry (TGA and DSC) under a nitrogen atmosphere show that the halide derivatives melt above 230 °C and decompose above 277 °C (5% weight loss).



**Scheme 1.** Preparation of copper CAAC halide and pseudo-halide complexes.

The  $^{\text{Me}2}\text{L}$  adducts  $(^{\text{Me}2}\text{L})\text{MX}$  have monomeric two-coordinate structures (Scheme 1), analogous to the more hindered  $(^{\text{Ad}}\text{L})\text{MX}$  compounds ( $M = \text{Cu}, \text{Au}$ ).<sup>[1,11]</sup> The structures of the series of compound with the slightly more bulky  $^{\text{Et}2}\text{L}$  ligand proved to be surprisingly sensitive to the subtle difference between the methyl and ethyl-substituted carbene ligands. For example, in the case of  $^{\text{Et}2}\text{L}$ , the reaction with  $\text{CuI}$  gave exclusively the ionic 2:1 complex,  $[(^{\text{Et}2}\text{L})_2\text{Cu}]\text{I}$ , irrespective of the  $^{\text{Et}2}\text{L}/\text{Cu}$  ratio. However, the otherwise inaccessible mono(carbene) iodide  $(^{\text{Et}2}\text{L})\text{CuI}$  could be obtained in high yields by halide exchange of  $(^{\text{Et}2}\text{L})\text{CuCl}$  with  $\text{NaI}$ .

Crystals of the copper halides suitable for X-ray diffraction were obtained by layering of  $\text{CH}_2\text{Cl}_2$  solutions with hexane. All compounds are monomeric with one molecule in the unit cell (see SI, Figure S24). Only weak intermolecular  $\text{C}-\text{H} \cdots \text{Hal}$  interactions were identified even in the case of the least-hindered  $(^{\text{Me}2}\text{L})\text{CuI}$  complex.

The structures of the  $\text{Cu}(\text{I})$  thiocyanates with  $^{\text{Me}2}\text{L}$  and  $^{\text{Et}2}\text{L}$  ligands differ significantly. The first indication that all complexes possess N-bound SCN ligand was provided by the nearly identical  $^{13}\text{C}$  NMR chemical shifts of  $(^{\text{Me}2}\text{L})\text{CuNCS}$  ( $\delta$  134.6),  $(^{\text{Et}2}\text{L})\text{CuNCS}$ , ( $\delta$  134.7) and  $(^{\text{Ad}}\text{L})\text{CuNCS}$  ( $\delta$  135.7), which agreed with previously reported N-bound thiocyanate complexes.<sup>[14]</sup> The IR stretching frequencies of  $(^{\text{Me}2}\text{L})\text{CuNCS}$  ( $2085 \text{ cm}^{-1}$ ) and  $(^{\text{Ad}}\text{L})\text{CuNCS}$  ( $2081 \text{ cm}^{-1}$ ) are consistent with N-bound terminal NCS

ligands, while the higher value observed for ( $^{Et_2L}$ )CuNCS ( $2111\text{ cm}^{-1}$ ) indicates bridging character.<sup>[15]</sup> These structures were confirmed by X-ray crystallography (Figure 1). ( $^{Me_2L}$ )CuNCS and ( $^{AdL}$ )CuNCS are monomeric, independent of the crystallisation conditions or the solvents used, with Cu–N–C bond angles of  $174.37(14)^\circ$  and  $171.50(13)^\circ$ , respectively. In contrast, the  $^{Et_2L}$  complex gave exclusively crystals of the N,S-bridged dimer, [ $^{Et_2L}$ ]Cu( $\mu,\kappa^2$ -NCS) $]$ <sub>2</sub>, with a distorted trigonal geometry around the two copper centres, which are related to each other by a crystallographic centre of inversion. Monomeric thiocyanates show N=C and C=S bond lengths of about  $1.162(2)$  and  $1.619(2)$  Å, whereas the N,S-bridged dimer is characterised by shorter C=N and longer C=S bonds ( $1.158(2)$  and  $1.659(2)$  Å), commensurate with a slight reduction of C-S double bond character in the dimer as indicated by infrared spectroscopy. In addition, in the three-coordinate complex the C<sub>carbene</sub>–Cu bond length is elongated by  $0.03$  Å.

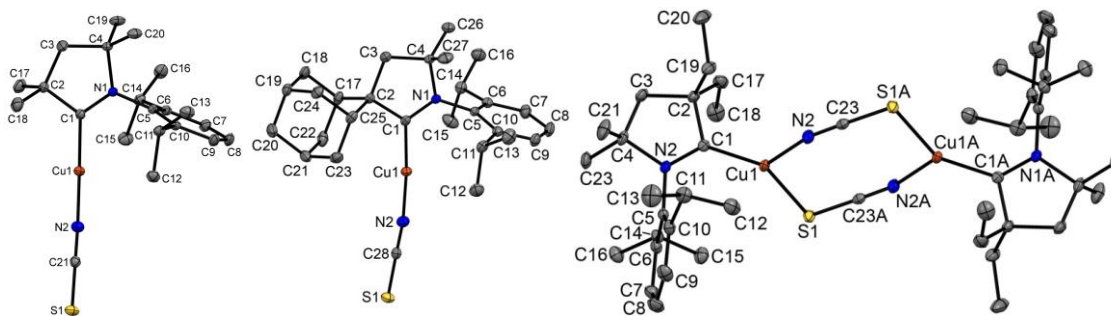


**Figure 1.** Crystal structures of copper thiocyanate complexes. Ellipsoids are shown at the 50% level. Hydrogen atoms are omitted for clarity. Selected bond lengths [Å] and angles [°]: ( $^{Me_2L}$ )CuNCS: Cu1–C1  $1.8715(14)$ , Cu1–N2  $1.8314(13)$ , C1–C2  $1.5164(19)$ , C1–N1  $1.3019(18)$ , N2–C21  $1.162(2)$ , C21–S1  $1.6190(15)$ ; C1–Cu1–N2  $174.10(6)$ , N2–C21–S1  $179.14(15)$ , Cu1–N2–C21  $174.37(14)$ . ( $^{AdL}$ )CuNCS: Cu1–C1  $1.8817(14)$ , Cu1–N2  $1.8297(13)$ , C1–C2  $1.5262(18)$ , C1–N1  $1.3011(17)$ , N2–C28  $1.161(2)$ , C28–S1  $1.6195(15)$ , C1–Cu1–N2  $174.96(6)$ , N2–C28–S1  $178.96(14)$ , Cu1–N2–C28  $171.50(13)$ . [ $^{Et_2L}$ ]CuNCS]<sub>2</sub>: Cu1–C1  $1.9024(12)$ , Cu1–N2  $1.9775(11)$ , Cu1–S1  $2.2881(4)$ , C1–C2  $1.5188(17)$ , C1–N1  $1.3129(15)$ , N2–C23  $1.1576(17)$ , C23–S1A  $1.6587(13)$ , C1–Cu1–N2  $124.22(5)$ , N2–C23–S1A  $178.73(11)$ , Cu1–N2–C23  $158.30(10)$ , S1–Cu1–N2  $102.33(3)$ . Symmetry operator (A):  $1 - x, 1 - y, -z$ .

Treating ( $^{AdL}$ )CuCl with an excess of KOH in dry THF containing a few drops of  $^i$ BuOH at room temperature for 36 h gave ( $^{AdL}$ )CuOH as a yellow powder (Scheme 2), which reacts with phenylacetylene in THF to give the acetylide, ( $^{AdL}$ )CuC<sub>2</sub>Ph, in excellent yield (see SI for crystallographic details of ( $^{AdL}$ )CuC<sub>2</sub>Ph). Neither the copper hydroxide nor the acetylide show significant photoluminescence.

*Gold halide and pseudo-halide complexes.* Attempts to synthesize gold bis(carbene) complexes using  $^{AdL}$  resulted in the exclusive formation of mono(carbene) products ( $^{AdL}$ )AuX. Gold pseudo-halides

with the adamantyl-substituted ligand, (<sup>Ad</sup>L)AuX, were prepared in quantitative yields by stirring a suspension of the known<sup>[11]</sup> chloride with KX (X = OCN, SCN, SeCN). Crystallographic and IR-spectroscopic studies unambiguously show that the cyanate is N-bonded ( $\nu_{\text{NCO}}$  2229  $\text{cm}^{-1}$ ), with an obtuse Au-N-CO angle of 158.2(2)°, while the thio- and selenocyanates are S/Se-bound ( $\nu_{\text{NCE}}$  2120/2125  $\text{cm}^{-1}$ ), with a more acute Au-S-CN angle of 103.3(2)° (Figure 2). Similar behaviour has been observed for the analogous LAu(pseudohalide) complexes with various donor ligands, e.g. L = thioether, phosphine, isocyanide,<sup>[15]</sup> or NHC.<sup>[16]</sup> The pseudo-halide complexes (<sup>Ad</sup>L)AuX are stable to ligand rearrangement in the solid or in CD<sub>2</sub>Cl<sub>2</sub> or CDCl<sub>3</sub> solutions; this contrast with reports on mixture of isomers with S- or N-coordinated SCN ligand for (<sup>t</sup>Bu<sub>2</sub>Im)AuSCN.<sup>[17]</sup> The (<sup>Ad</sup>L)AuX complexes are monomeric in the solid state and show weak intermolecular C–H···O or C–H···N interactions but no close Au···Au contacts. This differs from the behaviour of Schmidbauer's LAuSCN complexes (L = trimethylphosphine, xylyl or mesityl isocyanide), which form dimers or tetramers due to aurophilic interactions.<sup>[16]</sup>

By contrast, the reaction of <sup>Ei2</sup>L with gold(I) halides gives a mixture of mono- and bis(carbene) products. Using the sterically similar cyclohexenyl-substituted CAAC ligand, Bertrand et al. reported the exclusive formation of the ionic bis(carbene) complex.<sup>[10]</sup> However, reducing the reaction temperature to -78 °C allows the selective synthesis of (<sup>Ei2</sup>L)AuCl in high yield. Once formed, this complex proved stable in solution, i.e. in CD<sub>2</sub>Cl<sub>2</sub> there was no evidence for ligand rearrangement and formation of [Au(<sup>Ei2</sup>L)]<sub>2</sub><sup>+</sup> over a period of >24 h. The <sup>13</sup>C carbene-C resonance of (<sup>Ei2</sup>L)AuCl at  $\delta$  237.2 is characteristic for a mono(carbene) complex, whereas the resonance for bis(carbene) complexes is shifted downfield to  $\delta$  250 ppm.<sup>[10,11]</sup>

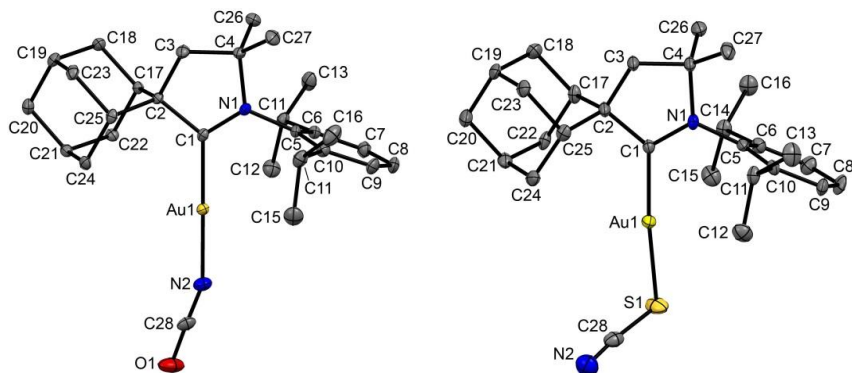
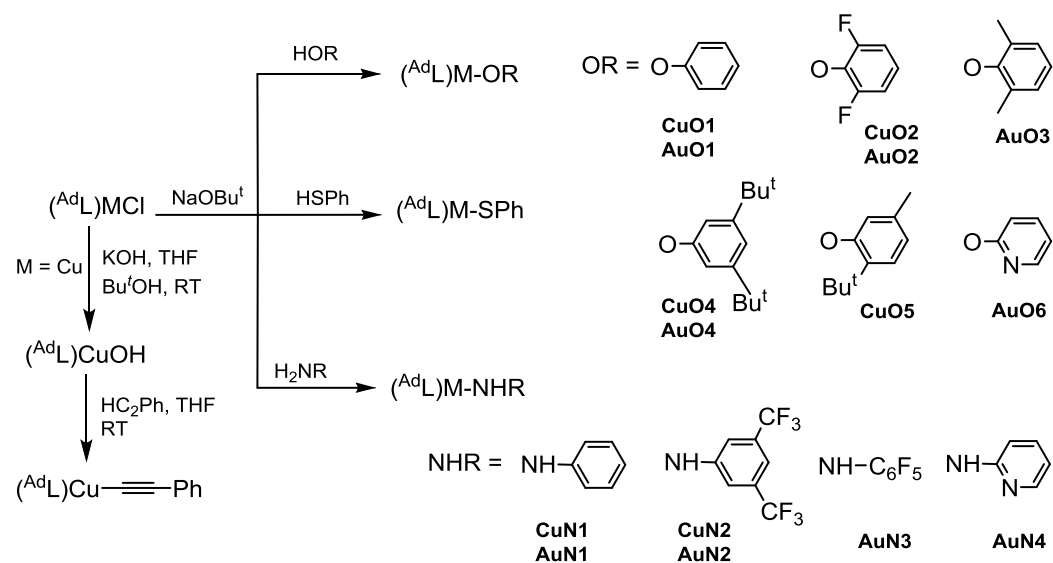


**Figure 2.** Crystal structures of (<sup>Ad</sup>L)AuNCO and (<sup>Ad</sup>L)AuSCN. Ellipsoids are shown at the 50% level. Hydrogen atoms are omitted for clarity. Selected bond lengths [Å] and angles [°]: (<sup>Ad</sup>L)AuNCO: Au1–C1 1.980(2), Au1–N2 2.004(2), C1–C2 1.535(3), C1–N1 1.308(3), N2–C28 1.164(3), C28–O1 1.199(3); C1–Au1–N2 179.23(8), N2–C28–O1 178.0(3), Au1–N2–C28 158.2(2). (<sup>Ad</sup>L)AuSCN: Au1–C1 2.011(6),

Au1–S1 2.3125(18), C1–C2 1.525(8), C1–N1 1.305(7), N2–C28 1.130(10), C28–S1 1.693(8); C1–Au1–S1 173.72(16), N2–C28–S1 174.5(7), Au1–S1–C28 103.3(2).

*Amido and phenolato complexes.* The reaction of (<sup>Ad</sup>L)MCl (M = Cu or Au) with phenols, thiophenol, or aromatic amines in the presence of NaO<sup>t</sup>Bu at room temperature in anhydrous THF provides a simple, high-yielding (>95%) route to the corresponding phenolato, thiophenolato and amido complexes (Scheme 2).<sup>[18]</sup> Complexes with Cu–O, Cu–S, Au–O and Au–S bonds are white or off-white. Gold amido compounds are yellow except those containing fluorinated aryl substituents, which are white solids, whereas the copper amido compounds are lime-green. These compounds show moderate to excellent solubility in most organic solvents but are only sparingly soluble in alkanes. Gold phenolates and thiolates are indefinitely stable in the solid state and in non-chlorinated solvents, whereas the copper compounds are air- and moisture-stable as solids for several days but decompose in chlorinated solvents. The stability of (<sup>Ad</sup>L)CuSPh contrast with reports on analogous NHC derivatives, e.g. (IMes)CuSPh which has been described as unstable and difficult to isolate.<sup>[19]</sup> The gold amides **AuN1** – **AuN4** are air-stable in the solid state and in solution, whereas copper compounds decompose in chlorinated solvents after several days.



**Scheme 2.** Synthesis of (<sup>Ad</sup>L)MX complexes

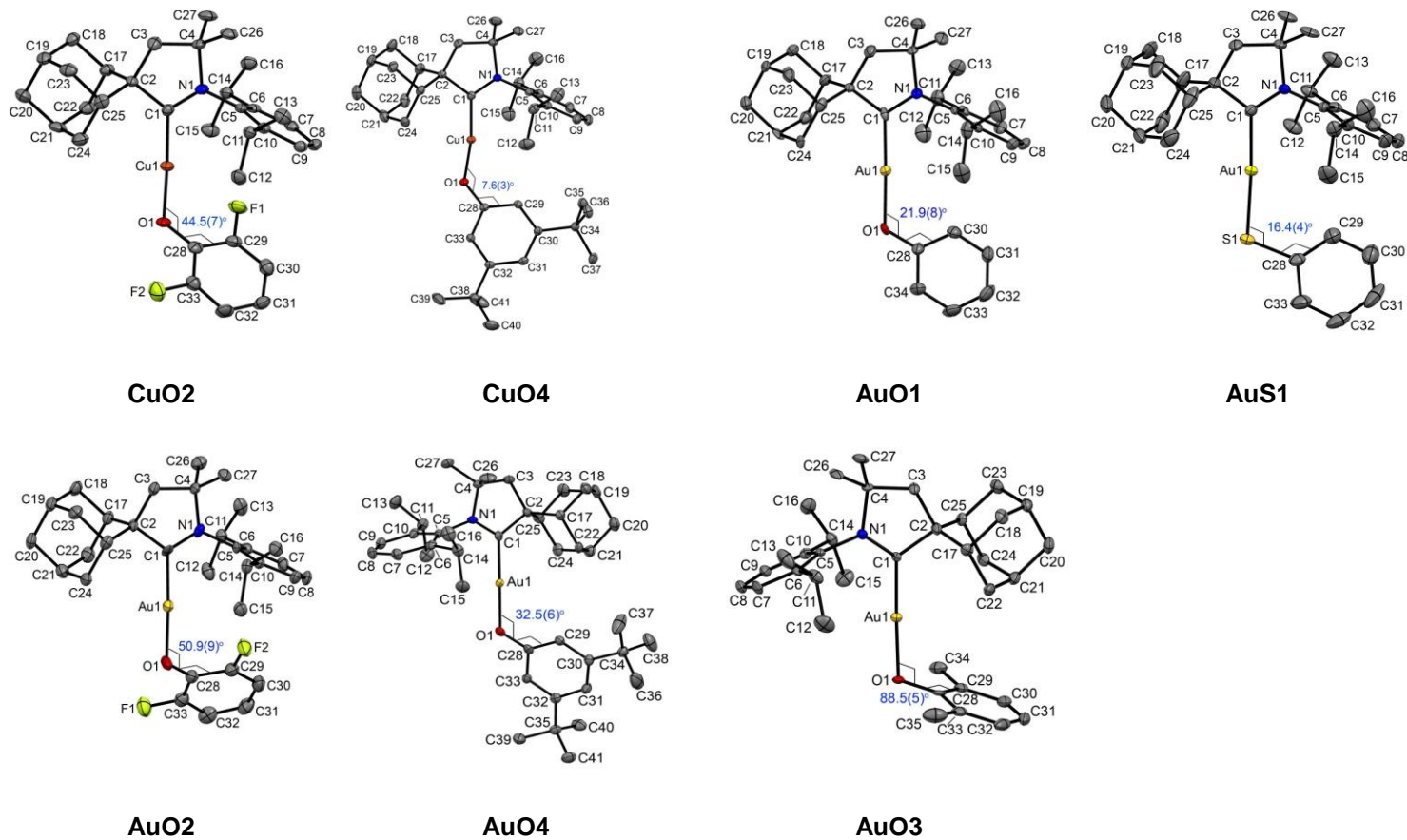


**Figure 3.** Crystal structures of CAAC metal aryloxides and the thiophenolate **AuS1**. Ellipsoids are shown at the 50% level. Hydrogen atoms are omitted for clarity. For structural parameters, see Table 1.

Representative crystal structures of metal aryloxides are shown in Figure 3. Compounds **CuO2** and **AuO1 – AuO4** crystallised with two independent molecules in the unit cell. The chosen crystal of **CuO4** contained one molecule of 3,5-Bu<sup>t</sup><sub>2</sub>C<sub>6</sub>H<sub>3</sub>OH which is O–H···O hydrogen-bonded to the Cu-OAr moiety and leads to a deviation from linearity around Cu, with a reduced Cu-O-C angle of 170.8° (see SI for details). Electron withdrawing fluorine substituents slightly elongate the C(carbene)–M and O1–Au bonds by 0.01 Å for **CuO2** and **AuO2** compared to other aryloxo complexes (Table 1). The structures of these compounds differ especially in the M-O-aryl torsion angles. *Ortho*-substituents on the aryloxo ligand favour a perpendicular orientation of the aryl substituent relative to the plane of the CAAC ligand. These structural variations appear to exercise a strong influence on the photoluminescence intensity of these complexes (*vide infra*).

**Table 1.** Selected bond lengths [Å] and angles [°] of copper and gold aryloxo complexes. The values for **CuO2** and **AuO1 – AuO4** are the averages of the two independent molecules in the unit cell.

Compd.	M-C1	M-O1	C1-C2	C1-N1	angle		torsion angle
					C1-M-O1	M-O1-C28-C29	
<b>CuO2</b>	1.868(4)	1.840(3)	1.538(6)	1.296(6)	173.54(19)	44.5(7)	
<b>CuO4</b>	1.8579(15)	1.8175(11)	1.529(2)	1.306(2)	170.78(6)	7.6(3)	
<b>AuO1</b>	1.966(6)	2.017(3)	1.538(8)	1.304(3)	176.9(3)	21.9(8)	
<b>AuO4</b>	1.962(4)	2.019(3)	1.536(6)	1.309(5)	179.37(15)	32.5(6)	
<b>AuO2</b>	1.977(5)	2.031(4)	1.534(8)	1.283(7)	178.2(2)	50.9(9)	
<b>AuO3</b>	1.965(5)	2.021(4)	1.545(7)	1.294(7)	178.1(2)	88.5(5)	
<b>AuS1</b>	2.006(4)	2.281(1)	1.537(5)	1.294(5)	176.3(1)	16.4(4)	

The crystal structures of copper and gold amido complexes **CuN2** and **AuN1 – AuN4** are monomeric, with a linear C(carbene)-M-N core. The complex (<sup>Ad</sup>L)AuNHPPh crystallizes as a solvate with 0.5 benzene which was disordered into two positions linked by twofold rotation axis with equal occupancies. Figure 4 shows the structures of **CuN2**, **AuN1**, **AuN2** and **AuN3**. A comparison of

geometric parameters is given in Table 2. The C<sub>4</sub>N-ring of carbene and the amido ligands are nearly coplanar. There is no electronic effect observed on the C(carbene)–Au bond length depending on the degree of fluoro substitution on anilide ligand, whereas gold-amide bond length N2–Au elongates by 0.02 Å in the order NPh < NH(3,5-C<sub>6</sub>H<sub>3</sub>(CF<sub>3</sub>)<sub>2</sub>) < NHC<sub>6</sub>F<sub>5</sub>. Although aurophilic interactions<sup>[20]</sup> are common in linear Au(I) complexes, none of metal aryloxo, thiophenolato, and amido compounds show close metal-metal contacts. In the fluorinated amides of copper and gold, two molecules are arranged to form dimers due to C–H···F hydrogen bonding, leading to spatially close N2–H2A and M atoms. The N2–H2A···M contact is longer than the sum of spherical van der Waals radii,<sup>[21]</sup> while metal-metal separation is in the range of 4.3 to 5 Å.

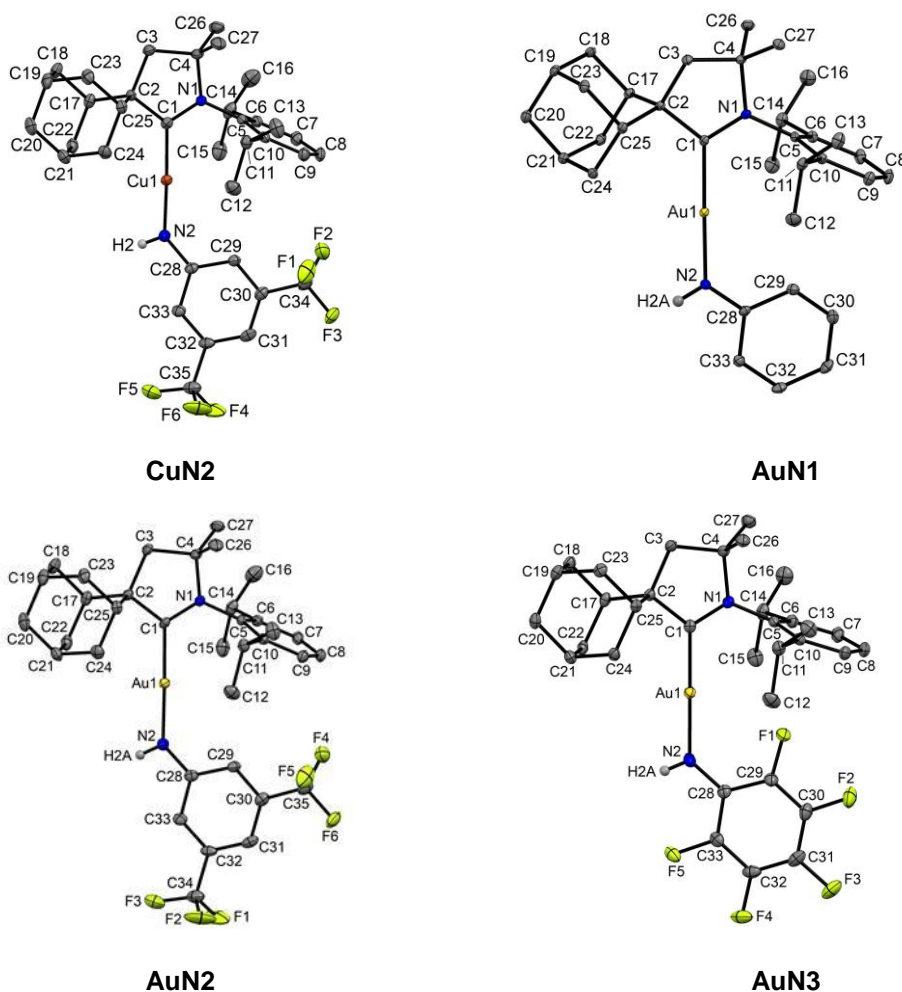


**Figure 4.** Crystal structures of copper and gold amido complexes **CuN2**, **AuN1**, **AuN2**, **AuN3**. Ellipsoids are shown at the 50% level. Hydrogen atoms are omitted for clarity.

**Table 2.** Selected bond lengths [ $\text{\AA}$ ] and angles [ $^\circ$ ] of copper and gold amido complexes.

Compd.	M-C1	M-N2	C1-C2	C1-N1	N2-C28	C1-M-N2
<b>CuN2</b>	1.879(2)	1.844(1)	1.530(2)	1.306(2)	1.359(2)	178.07(7)
<b>AuN1</b>	1.978(2)	1.996(2)	1.530(3)	1.313(3)	1.371(3)	178.70(7)
<b>AuN2</b>	1.983(3)	2.008(2)	1.531(3)	1.303(3)	1.349(3)	178.88(8)
<b>AuN3</b>	1.975(2)	2.017(2)	1.531(3)	1.311(3)	1.352(3)	179.55(8)

### Photoluminescence Properties.

*Luminescence of copper halide complexes.* The complexes under consideration here are linear monomers and contain strongly  $\sigma$ -donating carbene ligands, designed to raise the d-orbital energy levels. These compounds differ therefore from other types of photoluminescent copper complexes which are based on three- and four-coordinate geometries with  $\pi$ -acceptor ligands such as aryl phosphines, pyridines or other heterocyclic  $N$ -donors and often form polynuclear halide-bridged aggregates. In such cases the photophysical properties are dominated by metal-to-ligand charge-transfer (MLCT), ligand-to-ligand charge-transfer (LLCT) and metal-halide-to-ligand charge-transfer (M+X)LCT transitions.<sup>[5,22-27]</sup>

The ligands  $^{\text{Me}2}\text{L}$  and  $^{\text{Et}2}\text{L}$  themselves are only weakly emissive at room temperature but at 77 K show blue fluorescence at 452 and 435 nm, respectively (SI, Figure S1), with lifetimes of around 12 ns (Figure S2). The UV-vis spectra of the free carbenes (Figure S1) show the presence of a  $\pi$ - $\pi^*$  absorption at ca. 260 nm. In addition there is a low-intensity shoulder trailing to ca. 400 nm for both  $^{\text{Me}2}\text{L}$  and  $^{\text{Et}2}\text{L}$  carbenes; the low extinction coefficients (33 and 53  $\text{L mol}^{-1} \text{cm}^{-1}$  for  $^{\text{Me}2}\text{L}$  and  $^{\text{Et}2}\text{L}$ ) suggest that it originates from an  $n$ - $\pi^*$  absorption. This absorption tail is likely to contribute to the excitation of  $^{\text{Me}2}\text{L}$  and  $^{\text{Et}2}\text{L}$  carbene complexes.

We have analyzed the linear halide and pseudo-halide complexes to envisage the effect of steric protection imposed by the CAAC ligands on the absorption and emission properties. The low-energy bands in the UV/vis absorption spectra of the copper halide and pseudo-halide adducts of  $^{\text{Me}2}\text{L}$  and  $^{\text{Et}2}\text{L}$  are assigned to a  $(\sigma + \text{X})-\pi^*$  charge transfer, in analogy to the assignment of the corresponding absorptions in  $^{\text{Ad}}\text{L}$  and related copper halide complexes.<sup>[1,28]</sup> The absorptions are blue-shifted by 20-30 nm compared to the bands of their  $(^{\text{Ad}}\text{L})\text{CuX}$  analogues (Table 3).

On excitation with UV light ( $\lambda_{\text{exc}} = 365 \text{ nm}$ ) the crystalline  $^{\text{Me}2}\text{L}$  and  $^{\text{Et}2}\text{L}$  copper halides display very broad white ( $^{\text{Me}2}\text{LCuX}$ ) and blue-white ( $^{\text{Et}2}\text{LCuX}$ ) emissions, ranging from 375 to 650 nm (half-width 6300 - 6500  $\text{cm}^{-1}$ ) (Figure 5) (for the excitation spectrum and emission spectra at various excitation

wavelengths see SI, Figure S4). The emission wavelengths are slightly halide-dependent and show a red shift of *ca.* 20 nm in the sequence X = Cl > Br  $\approx$  I (Table 3). All sublimed ( $^{R2}L$ )Cu complexes show intense triboluminescence.

The photoemissions of ( $^{Ad}L$ )CuX type complexes had been evaluated over a temperature range of 4 – 300 K and found to be caused by very fast prompt fluorescence.<sup>[1]</sup> The  $^{Me2}L$  and  $^{Et2}L$  complexes reported here showed similar behavior in the nanosecond range: monitoring the emissions using time-correlated single photon counting (TCSPC) shows short emission lifetimes (limited by the response time of the instrument used of  $\sim 2$  ns), typical of prompt fluorescence. However, at the microsecond range it was possible to detect both short- and long-lived components (Figure 5 and SI, Figures S8).<sup>[29]</sup>

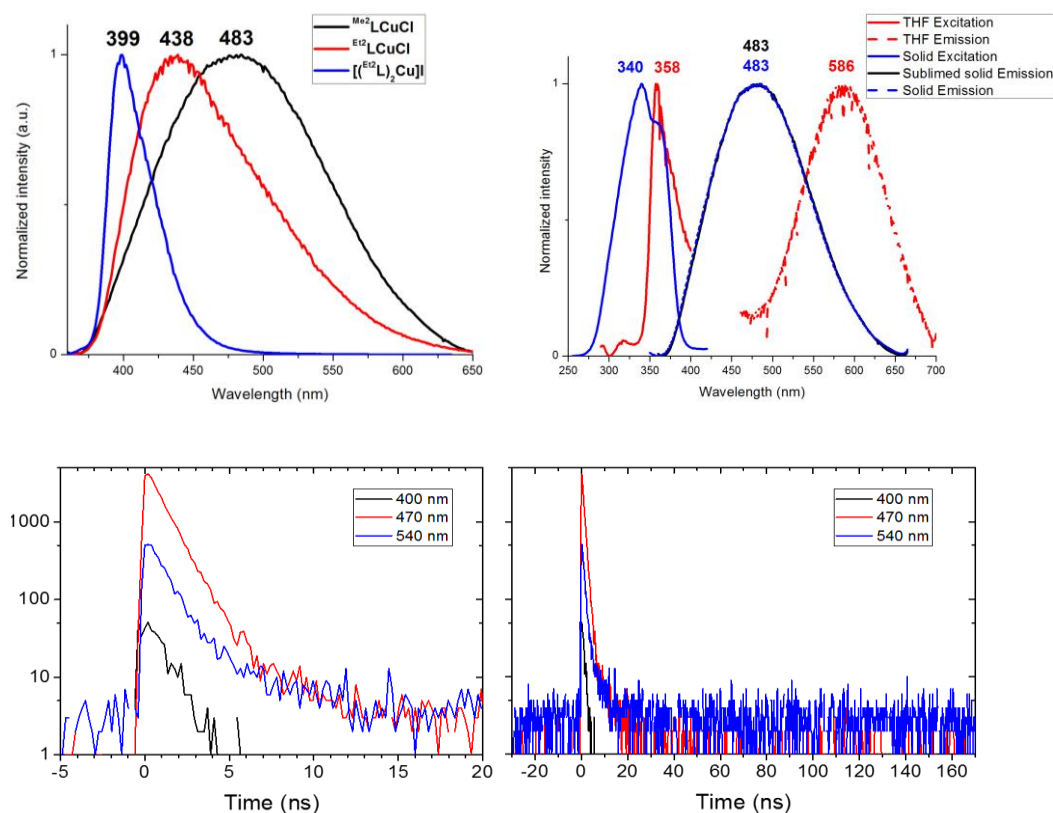


**Figure 5.** Top left: emission spectra of ( $^{Me2}L$ )CuCl, ( $^{Et2}L$ )CuCl and  $[(^{Et2}L)_2Cu]I$  in the solid state ( $\lambda_{ex}$  330 – 370 nm). Top right: excitation and emission spectra for ( $^{Me2}L$ )CuCl as solid and in THF solution. The spectra of freshly isolated and sublimed samples of ( $^{Me2}L$ )CuCl are superimposable. Bottom: Emission kinetics of ( $^{Me2}L$ )CuCl on two time axes, measured using a 407 nm picosecond pump and a monochromated TCSPC detector operating at 5 MHz. Scattering was removed by applying a 435 nm long-pass filter. The decay lifetime is approximately 1 ns. The IRF is measured at 500 nm from a scattering sample and is approximately 200 ps wide.

Sample purity is paramount for the evaluation of the photoemissions. Compared to the  ${}^{\text{Ad}}\text{L}$  complexes reported earlier,<sup>[1]</sup> the  ${}^{\text{Me}2}\text{L}$  and  ${}^{\text{Et}2}\text{L}$  copper halide complexes are more sensitive and prone to photo-degradation by ambient light or, much faster, by UV or laser irradiation. Samples were routinely purified by filtration of dichloromethane solutions through silica, and/or by sublimation. The PL spectra of silica-purified and sublimed samples were superimposable. On the other hand, traces of a component with longer-lived emission could not be entirely eliminated, and photodegradation of  $({}^{\text{Me}2}\text{L})\text{CuCl}$  increases the intensity of the long-lived component with  $\mu\text{s}$  life time. (see SI, Figures S10, S11). Subliming samples prepared without silica filtration left traces of unknown beige impurities, which enhanced the intensity of the  $\mu\text{s}$ -emission.

For the crystalline complexes, the quantum yields increase with increasing bulkiness of the carbene ligand in the sequence  ${}^{\text{Me}2}\text{L} < {}^{\text{Et}2}\text{L} < {}^{\text{Ad}}\text{L}$ , in consequence of the increasing rigidity of the molecular system (for the optimized geometries of  $({}^{\text{Me}2}\text{L})\text{CuCl}$  and  $({}^{\text{Ad}}\text{L})\text{CuCl}$  in the  $\text{S}_1$  and  $\text{T}_1$  excited states see SI, Figure S15). The gold halide  $({}^{\text{Et}2}\text{L})\text{AuCl}$  is non-emissive, in contrast to  $({}^{\text{Et}2}\text{L})\text{CuCl}$  and its bulkier analogue  $({}^{\text{Ad}}\text{L})\text{AuCl}$ .

In solution the copper halide complexes are only weakly emissive, and the luminescence is red-shifted (Figure 5, and SI, Table S1 and Figures S5, S7 and S9). As we have shown before,<sup>[1]</sup> this points to emissions from solvent exciplexes, with >90% of the emission being due to slow components with lifetimes of 300-800 ns, which increases with increasing steric protection of the metal centre  $({}^{\text{Me}2}\text{L})\text{Cu} < ({}^{\text{Et}2}\text{L})\text{Cu} \approx ({}^{\text{Ad}}\text{L})\text{Cu}$ . In the presence of oxygen this exciplex emission is effectively quenched, as expected for the involvement of triplet states.

The UV/vis spectra of the bis(carbene) compounds  $[({}^{\text{Me}2}\text{L})_2\text{Cu}]\text{I}$  and  $[({}^{\text{Et}2}\text{L})_2\text{Cu}]\text{I}$  show MLCT bands at 320 nm. Unlike the mono(carbene) complexes,  $[({}^{\text{Et}2}\text{L})_2\text{Cu}]\text{I}$  exhibits a very narrow fluorescence profile in the violet region of the spectrum, with a half-width of only  $2200\text{ cm}^{-1}$ .

Shortly before the submission of this manuscript a publication appeared which claimed that  $({}^{\text{Me}2}\text{L})\text{CuX}$  and  $[({}^{\text{Me}2}\text{L})_2\text{Cu}]^+$  complexes show only phosphorescence, with emission lifetimes of tens of microseconds.<sup>[13]</sup> Here we show that more than one emission mechanism operates, i.e. prompt emission in the nanosecond range, together with a minor component with microsecond life time. Careful comparison with the emission spectra of free carbenes allows us to rule out the formation of free ligand as the source of fluorescence. It also became evident that sample handling and photodegradation of  $({}^{\text{Me}2}\text{L})\text{CuX}$  complexes leads to an increase in the intensity of the long-lived component (see SI, Figures S10, S11).<sup>[30]</sup>

Our assignments were further confirmed by density functional theory (DFT) and time-dependent DFT calculations of the ground and excited state geometries of  $({}^{\text{R}}\text{L})\text{CuCl}$  complexes. Whereas the relaxed  $\text{S}_1$  state of  $({}^{\text{Ad}}\text{L})\text{CuCl}$  is nearly identical to the  $\text{S}_0$  ground state,<sup>[1]</sup> the  $\text{S}_1$  structure of  $({}^{\text{Me}2}\text{L})\text{CuCl}$  shows

significant distortion in the N-C-Cu and C-Cu-Cl angles, which affects its fluorescence properties (see SI, Figure S15). The  $S_1$  states lie 2.96 and 3.11 eV above  $S_0$  for ( $^{Ad}L$ )CuCl and of ( $^{Me_2}L$ )CuCl, respectively. Fluorescence taking place from  $S_1$  to  $S_0$  with nuclei fixed in  $S_1$  geometry gives energy differences of 2.72 eV (456 nm) for ( $^{Ad}L$ )CuCl and 2.58 eV (480 nm) for ( $^{Me_2}L$ )CuCl, in excellent agreement with the observed emissions at  $\lambda_{em} = 453$  nm and 483 nm for the  $^{Ad}L$  and  $^{Me_2}L$  complexes, respectively. Relaxed  $T_1$  states show similar distortion for ( $^{Me_2}L$ )CuCl and no distortion for ( $^{Ad}L$ )CuCl and lie 2.57 and 2.76 eV, respectively, above  $S_0$ . The energy differences between relaxed  $T_1$  and  $S_0$  with nuclei fixed in  $T_1$  geometry for phosphorescence are 2.30 eV (538 nm, ( $^{Ad}L$ )CuCl) and 2.06 eV (602 nm, ( $^{Me_2}L$ )CuCl), which may contribute to the broadness of the emission band.

*Luminescence of copper thiocyanate complexes.* The structural differences in copper thiocyanates (*vide supra*) are reflected in the photoluminescence properties of these compounds: monomeric, two-coordinate ( $^{Me_2}L$ )CuNCS is a weak white emitting material ( $\lambda_{em} = 402$  nm, PLQY 4%) while dimeric, three-coordinate [ $(^{Et_2}L)Cu(\mu-NCS)$ ] $_2$  shows intense yellow luminescence ( $\lambda_{em} = 553$  nm, QY 49%), which is dominated by a slow component with a lifetime of 453 ns (at 300 K) (Figure 6). The emission profile of ( $^{Me_2}L$ )CuNCS possesses a shoulder at ca. 520 nm, which suggests the presence of a small fraction of dimeric species of [ $(^{Me_2}L)CuNCS$ ] $_2$  in the bulk material. The more sterically hindered ( $^{Ad}L$ )CuNCS shows featureless blue emission ( $\lambda_{em} = 429$  nm, QY 31%), indicating that the bulk material contains only monomeric species. Unlike copper thiocyanates, gold pseudo-halides are only very weakly emissive.

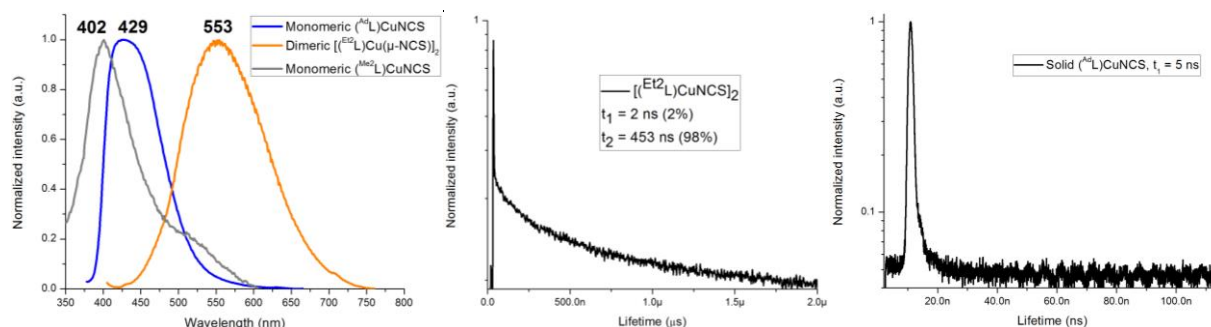


**Figure 6.** Emission spectra of ( $^{Me_2}L$ )CuNCS ( $\lambda_{ex} = 324$  nm), ( $^{Ad}L$ )CuNCS ( $\lambda_{ex} = 351$  nm) and [ $(^{Et_2}L)Cu(\mu-NCS)$ ] $_2$  ( $\lambda_{ex} = 392$  nm) in the solid state (left) and time-resolved photoluminescence decay of dimeric [ $(^{Et_2}L)CuNCS$ ] $_2$  and monomeric ( $^{Ad}L$ )CuNCS ( $\lambda_{ex} = 370$  nm).

*Luminescence of phenolato and amido complexes.* The UV/vis absorption spectra of the copper and gold aryloxides and thiolates complexes in THF solutions (Figure 7) show two absorptions below 300 nm due to an intra-ligand transition of the CAAC ligand, similarly to those observed for analogous halide complexes (Tables 3 and 4). Additionally, an intense absorption band spanning from 320 to 400 nm

(Figures 7) is ascribed to ligand-metal-ligand charge-transfer (LMLCT), with a contribution of the metal atom. Relative to the unsubstituted complex **CuO1**, the LMLCT band for the 2,6-difluoro substituted complex **CuO2** shifts by 26 nm to higher energies, whereas there is a 10 nm red-shift for the thiolate (<sup>Ad</sup>L)CuSPh and the methyl-substituted aryloxides **CuO4** and **CuO5**. This is evidently a reflection of the electron withdrawing (**CuO2**) and electron-donating properties of the aryloxide ligands.

The gold complexes show similar UV-vis spectra, which further supports the assignment of the absorption band at 350 nm to LMLCT with a contribution of the metal atom, which was supported by DFT calculations on the changes in electron distribution in the  $S_0$  and  $S_1$  states (Figure 8 and SI, Figures S16 and S17).

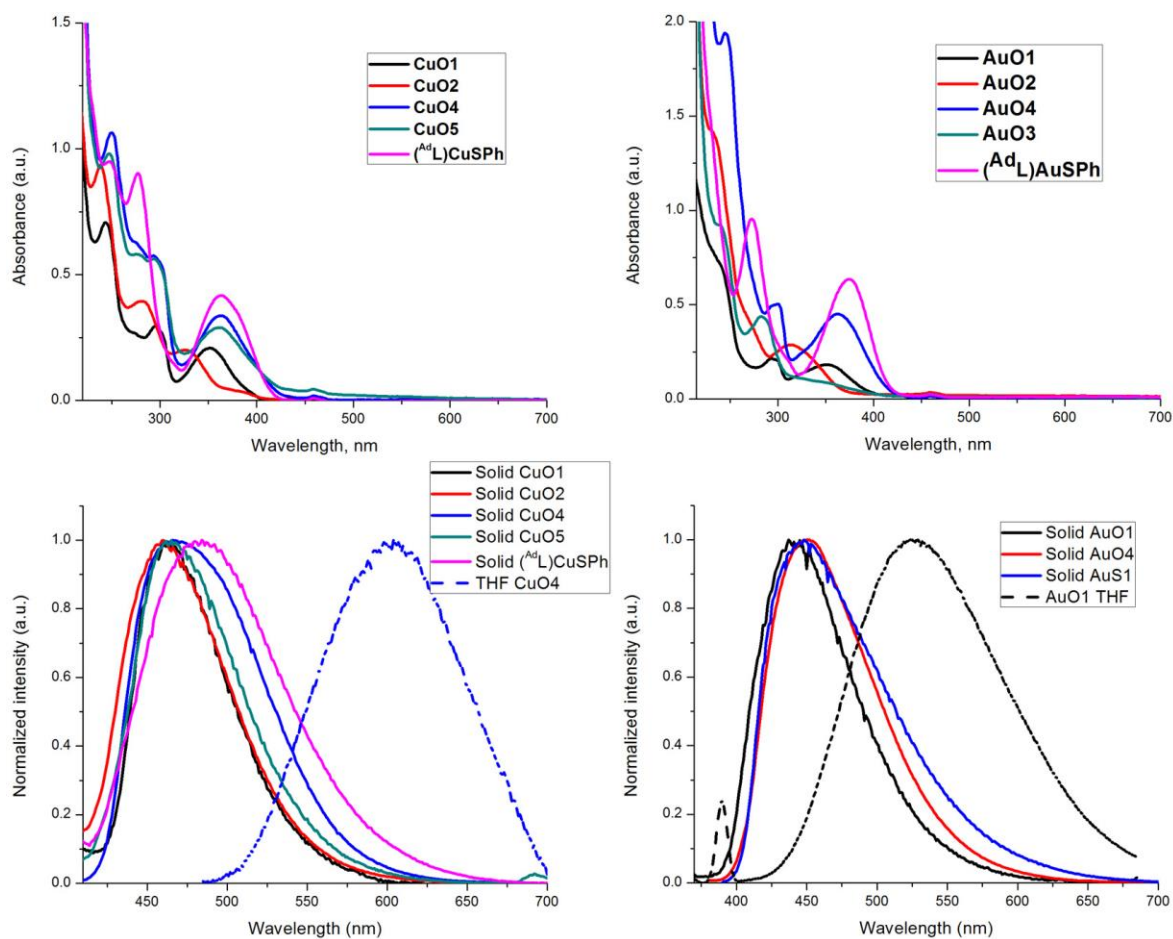


**Figure 7.** Top: UV-vis spectra for THF solutions of phenolate and thiophenolate complexes of copper (left) and gold (right). Bottom: Photoluminescence spectra of copper phenolates **CuO1-O5** and of (<sup>Ad</sup>L)CuSPh in the solid state and THF (left) and analogous gold complexes (right) state ( $\lambda_{ex}$  370 nm).

The copper and gold phenolates are blue emitters, whereas the thiolates emit in the blue-green region. The PL properties of the copper aryloxides are largely unaffected by shifts of the LMLCT band, i.e. the emission energy is independent of the donor or acceptor characteristics of the aryl substituents. The solution behavior of copper and gold phenolate complexes is very similar to halides (L)M(X): the emission maxima are significantly red-shifted by 100 nm, while solutions become very poorly emissive (Figure 7).

**Table 3.** Photophysical properties of copper complexes (298 K)

Complex	Absorption/nm ( $10^3 \epsilon/M^{-1} \text{ cm}^{-1}$ ) in deaerated THF	Solid state				
		$\lambda_{\text{em}} (\lambda_{\text{ex}})$ (nm)	$\tau^a$	$\Phi^b$	$k_r$ ( $10^5 \text{ s}^{-1}$ ) <sup>c,e</sup>	$k_{\text{nr}}$ ( $10^5 \text{ s}^{-1}$ ) <sup>d,e</sup>
$\text{Me}_2\text{L}$	260 (0.58), 310 sh 0.03)	452 (290–380)	12.2±0.2 ns	n.d.	n.d.	n.d.
$(\text{Me}_2\text{L})\text{CuCl}$	282 (10.0), 333 (1.0)	483 (290–380)	7.0±0.4 ns 8.3±0.4 $\mu\text{s}$	0.22	0.27	0.95
$(\text{Me}_2\text{L})\text{CuBr}$	283 (4.4), 326 (1.7)	488 (290–380)	4.4±0.4 17.1±0.4 $\mu\text{s}$	0.36	0.21	0.38
$(\text{Me}_2\text{L})\text{CuI}$	291 (9.6), 322 (2.5)	508 (290–380)	2.0±0.2 ns 8.7±0.1 $\mu\text{s}$	0.24	0.28	0.89
$(\text{Me}_2\text{L})\text{CuNCS}$	244 (17.4), 291 (16.5), 324 (sh, 1.8)	402 (290–370)	3.4±0.1 ns 2.4±0.1 $\mu\text{s}$	0.04	0.17	4.0
$[(\text{Me}_2\text{L})_2\text{Cu}]\text{I}$	248 (27.8), 266 (sh, 16.6), 330 (2.4), 343 (2.2)	390, 454 (290– 370)	3.3±0.1 ns 5.4±0.1 $\mu\text{s}$	0.14	0.26	1.6
$\text{Et}_2\text{L}$	262 (1.0), 310 sh (0.05)	435 (270–370)	12.7±0.3 ns	n.d.	n.d.	n.d.
$(\text{Et}_2\text{L})\text{CuCl}$	282 (6.4), 335 (0.8)	437 (290–380)	3.2±0.1 ns 25.7±0.2 $\mu\text{s}$	0.70	0.27	0.11
$(\text{Et}_2\text{L})\text{CuBr}$	283 (7.3), 332 (0.6)	461 (290–380)	2.5±0.1 ns 19.8±0.2 $\mu\text{s}$	0.48	0.24	0.26
$(\text{Et}_2\text{L})\text{CuI}$	289 (7.6), 336 (0.9)	486 (280–400)	3.0±0.1 ns 15.8±0.4 $\mu\text{s}$	n.d.	n.d.	n.d.
$[(\text{Et}_2\text{L})\text{CuNCS}]_2$	244 (0.8), 291 (0.7), 324 (0.1)	553 (300–440)	2.0±0.1 (2%) ns 453±7 (98%) ns	0.49	0.01	0.012
$[(\text{Et}_2\text{L})_2\text{Cu}]\text{I}$	258 (15.4), 329 (1.3)	399 (280–390)	2.1±0.1 ns 8.5±0.1 $\mu\text{s}$	0.37	0.44	0.75
$(\text{AdL})\text{CuNCS}$	297 (11.7), 354 (0.4)	429 (290–410)	2.7±0.1 ns 7.5±0.2 $\mu\text{s}$	0.31	0.42	0.93
<b>CuO1</b>	244 (7.5), 295 (3.1), 352 (2.2)	467 (300–450)	2.0±0.5 (4%) ns 472±10 (96%) ns	0.57	12	9
<b>CuO2</b>	238 (10.6), 281 (4.4), 326 (2.2), 370 (sh, 0.5)	460 (381)	2.0±0.5 (5%) ns 585±20 (95%) ns	0.22	4	12
<b>CuO4</b>	247 (7.3), 279 (4.1), 290 (3.8), 362 (1.6)	466 (300–450)	2.0±0.1 (2%) ns 660±27 (98%) ns	0.57	8	6
<b>CuO5</b>	250 (12.1), 285 (6.4),	465 (300–450)	2.0±0.5 (4%) ns	0.38	8	3

	362 (3.8)		458±7 (96%) ns			
( <sup>Ad</sup> L)CuSPh	248 (7.3), 277 (6.9), 363 (3.2)	484 (300–425)	2.0±0.5 (2%) ns 506±12 (98%) ns	0.62	12	7
<b>CuN1</b>	240 (15.6), 291 (6.5), 342 (2.2), 408 (sh, 1.0)	500 (300–470)	9.7±0.4 (1.5%) ns 455±5 (98.5%) ns	0.11	2.4	19.9
<b>CuN2</b>	251 (9.6), 291 (9.2), 366 (5.2)	513 (300–450)	6±0.3 (4%) ns 288±7 (96%) ns	0.045	1.5	33.7

<sup>a</sup> Excited state lifetime, measured at  $\lambda_{\max}$ ; <sup>b</sup> Quantum yields determined by using an integrated sphere; <sup>c</sup> radiative rate constant  $k_r = \Phi/\tau$ ; <sup>d</sup> Nonradiative constant  $k_{nr} = (1 - \Phi)/\tau$ ; <sup>e</sup> in case of two-component lifetime  $\tau$  average was used:  $\tau_{av} = (B_1/(B_1 + B_2))\tau_1 + (B_2/(B_1 + B_2))\tau_2$ , where  $B_1$  and  $B_2$  are relative amplitude for  $\tau_1$  and  $\tau_2$ , respectively.

**Table 4.** Photophysical properties of gold complexes (298 K)

Complex	Absorption/nm ( $10^3$ $\varepsilon/M^{-1} \text{ cm}^{-1}$ ) in THF	Solid state				
		$\lambda_{em} (\lambda_{ex})$ (nm)	$\tau^a$ (ns)	$\Phi^b$	$k_r (10^5$ $s^{-1})^{c,e}$	$k_{nr} (10^5$ $s^{-1})^{d,e}$
<b>AuO1</b>	236 (4.9), 293 (1.4), 350 (1.2)	447 (300– 400)	37.6±0.1 (6%) 129.7±0.1 (94%)	0.02	2	80
<b>AuO2</b>	228 (15.9), 268 (4.9), 314 (3.1)	–	–	–	–	–
<b>AuO3</b>	237 (10.2), 283 (4.8), 326 (1.1)	–	–	–	–	–
<b>AuO4</b>	245 (27.3), 300 (7.0), 362 (6.3)	449 (290– 420)	2.0±0.1 (0.5%) 316±5 (99.5%)	0.47	15	17
( <sup>Ad</sup> L)AuSPh	273 (9.5), 375 (6.3)	448 (300– 420)	4±0.6 (10%) 255±2 (90%)	0.26	11	32
<b>AuN1</b>	275 (8.4), 327 (3.3), 429 (7.2)	506 (300– 475)	7.7±0.8 (1.5%) 275±10 (98.5%)	0.38	14	29
<b>AuN2</b>	215 (17.2), 283 (9.0), 364 (7.2), 372 (6.9)	493 (300– 450)	4.4±0.1 (19%) 117±7 (81%)	0.13	14	91
<b>AuN3</b>	253 (10.2), 360 (6.0)	–	–	–	–	–
<b>AuN4</b>	266 (15.3), 334 (6.3), 391 (13.4)	491 (300– 450)	5±0.4 (2%) 264±14 (98%)	0.06	2	36

<sup>a</sup> Measured at  $\lambda_{\max}$ ; <sup>b</sup> Quantum yields determined by using an integrated sphere; <sup>c</sup> radiative rate constant  $k_r = \Phi/\tau$ ; <sup>d</sup> Nonradiative constant  $k_{nr} = (1 - \Phi)/\tau$ . <sup>e</sup> in case of two-component lifetime  $\tau$  average was used:  $\tau_{av} = (B_1/(B_1 + B_2))\tau_1 + (B_2/(B_1 + B_2))\tau_2$ , where  $B_1$  and  $B_2$  are relative amplitude for  $\tau_1$  and  $\tau_2$ , respectively.

The emission intensities of copper complexes bearing substituents in *ortho*-positions on the phenol ring are generally weaker than for unsubstituted or *meta*-substituted derivatives. For instance, compounds

**CuO2** and **CuO5** show PLQY values reduced to 22 and 38%, respectively, compared to a PLQY of 57% for the unsubstituted **CuO1** and *m*-disubstituted **CuO4**.

The emissions of the copper and gold aryloxides are dominated by a delayed process, with a lifetime of several hundreds of ns and quantum yields of up to 57%, leading to a radiative rate constant of ca.  $8 \times 10^5 \text{ s}^{-1}$  (Tables 3 and 4 and SI, Figure S14). The detrimental effect of *ortho*-substituents on the phenolate rings is particularly pronounced for gold complexes **AuO2** and **AuO3**, whose emissions are completely quenched. Within the series of gold phenolates, this trend in solid state emission intensities seems to correlate with the structural features of these compounds. The torsion angles Au1–O1–C28–C29 increase in the order **AuO1** ( $21.5^\circ$ ) < **AuO4** ( $32.5^\circ$ ) < **AuO2** ( $50.9^\circ$ ) < **AuO3** ( $88.5^\circ$ ). Only the first two complexes with torsion angles  $< 50^\circ$  are emissive, whereas larger angles lead to quenching. **AuO1** and **AuO4** are blue emitters.

DFT calculations show that in the optimised  $S_0$  state, the CAAC 5-ring and the OPh ligand are coplanar. Electron density calculations confirmed the LMLCT nature of the  $S_0 \rightarrow S_1$  transition, which leads to significant polarity changes in the molecules (Figure 8). The torsion angles are apparently imposed by crystal packing forces. As Figure 9 shows, the oscillator strength decreases as the aryl oxide ligand is rotated from  $0^\circ$  to  $90^\circ$ , in agreement with the PL behaviour of the gold aryloxides.

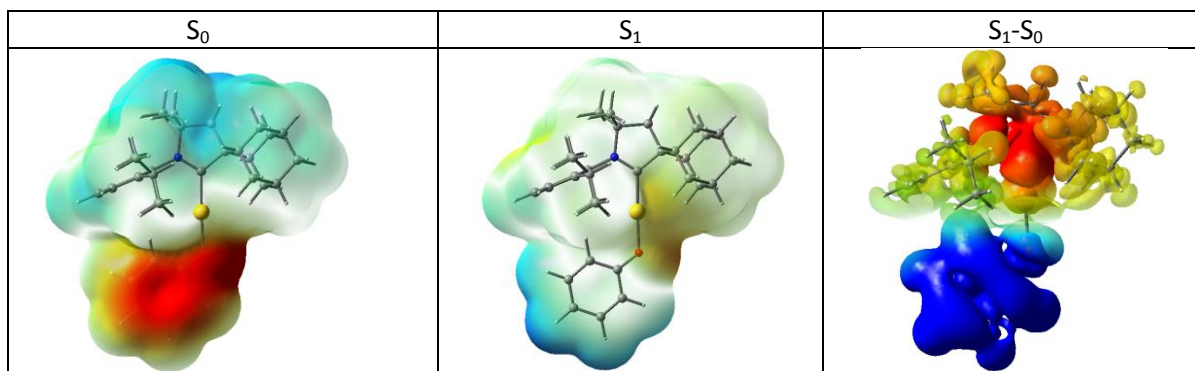


**Figure 8.** Electron density distribution of **AuO1** in the  $S_0$  and  $S_1$  states, and the difference in electron distribution during the  $S_0 \rightarrow S_1$  transition. Red and blue illustrate areas of high and low electron density, respectively.

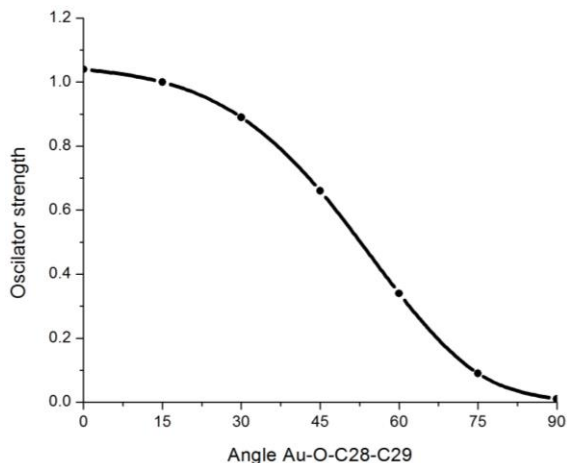


**Figure 9.** Oscillator strength of **AuO1** as a function of the Au-O-C-C torsion angle of the OPh ligand relative to the best plane of the CAAC 5-ring.

The PL intensities of **AuO1** – **AuO4** correlate well with the calculated oscillator strengths for these geometries (Table 5), except for the *o*-F<sub>2</sub> derivative **AuO2** which expectedly has a much larger excitation energy due to electron withdrawing substituents. Apart from photoluminescence, all the copper and gold aryloxides and thiolates show intense blue triboluminescence in the solid state.

**Table 5.** S<sub>0</sub> → S<sub>1</sub> excitation energies and relative oscillator strengths in crystal structure geometries:

Complex	S <sub>1</sub> -S <sub>0</sub> / eV	Oscillator strength
<b>AuO1</b>	2.85	0.96
<b>AuO2</b>	3.24	0.55
<b>AuO3</b>	2.87	0.01
<b>AuO4</b>	2.68	1.00

The CAAC copper and gold amides are green emitters under excitation with UV light at 365 nm. The normalised PL decay curves (Figure 10 and SI, Figure S14) indicate that the emission has a minor prompt fluorescence component in the range of several ns and major delayed component of several hundred ns. The PLQYs reduce significantly with increasing degree of fluorination of aniline ligand. For instance, the pentafluoroanilide complex **AuN3** is completely non-emissive.

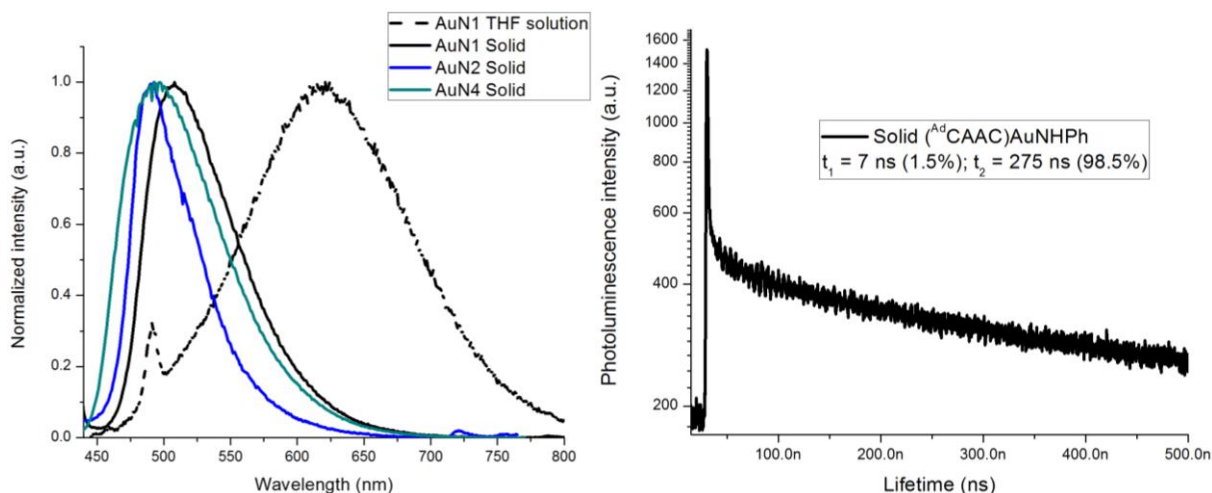


**Figure 10.** Left: Solid state emission spectra of **AuN1**, **AuN2**, **AuN4** and of **AuN1** in THF solution. Right: Example of the time-resolved photoluminescence decay of **AuN1** in the solid state ( $\lambda_{\text{ex}}$  370 nm).

### Electrochemistry

Cyclic voltammetry (CV) was used to analyse the redox behaviour of the CAAC copper and gold complexes in MeCN solution using  $[\text{Bu}_4\text{N}]\text{PF}_6$  as the supporting electrolyte (Table 6). The mono(carbene) copper halides ( $\text{X} = \text{Cl}$  and  $\text{Br}$ ) undergo one metal-centred one-electron irreversible reduction process. A re-oxidation peak could not be detected at all scan rates from 0.05 to  $2 \text{ Vs}^{-1}$ , while the peak maximum clearly shifts with the applied voltammetric scan rate. Unlike other carbene halide complexes, the copper pseudo-halide and the iodide ( $^{\text{Me}2}\text{L}$ )CuI show two irreversible reduction processes while no back-peaks are observed for both reductions (see SI, Figure S21). The reduction process of copper thiocyanate complexes is largely broadened and was resolved into two reduction processes only in the case of ( $^{\text{Ad}}\text{L}$ )CuNCS.

The ionic bis(carbene) complexes  $[(^{\text{R}}\text{L})_2\text{Cu}]\text{I}$  show a quasi-reversible one-electron reduction process (see SI, Figure S22) with a significant anodic shift of the reduction potential  $E_{1/2}$  by 0.3 V compared to mono(carbene) chloride complexes (see Table 6). The one-electron character of the reduction process was inferred by the calculation of the number of the electrons using the Randles–Ševčík equation for a quasi-reversible system for the cationic complex  $[(^{\text{Et}}\text{L})_2\text{Cu}]\text{I}$  (see SI for calculations and plots of peak current vs scan rate, Figure S18). The quasi-reversibility of the reduction peak is witnessed by the negligible shift of 10 mV in the peak position  $E_p$  on increasing the scan rate and the peak-to-peak separation  $\Delta E_p$  of 70 mV (at 100 mV/s), which is close to the ideal value of 59 mV for a one-electron reversible couple. Also,  $[(^{\text{Et}2}\text{L})_2\text{Cu}]\text{I}$  shows that the  $i_{\text{pa}}/i_{\text{pc}}$  ratio increases from 0.32 (at  $50 \text{ mVs}^{-1}$ ) to 0.75 (at  $2 \text{ Vs}^{-1}$ ) and is approaching unity, which is the ideal value for a reversible couple (SI, Figure S19). The analogous  $^{\text{Me}2}\text{L}$  complex  $[(^{\text{Me}2}\text{L})_2\text{Cu}]\text{I}$ , with a less bulky ligand, shows an irreversible reduction process at

low scan rates (50 to 250  $\text{Vs}^{-1}$ ) which becomes quasi-reversible at higher scan rates (0.5 to 2  $\text{Vs}^{-1}$ , see SI, Figure S22). Therefore, the bulkier CAAC ligands exert only a marginal effect on the peak position of the redox processes but increase the quasi-reversible character of the reduction process.

**Table 6.** Formal electrode potentials (peak position  $E_p$  for irreversible and  $E_{1/2}$  for quasi-reversible processes (\*), V, vs.  $\text{FeCp}_2$ ), onset potentials ( $E$ , V, vs.  $\text{FeCp}_2$ ), peak-to-peak separation in parentheses for quasi-reversible processes ( $\Delta E_p$  in mV),  $E_{\text{HOMO}}/E_{\text{LUMO}}$  (eV) and band gap values ( $\Delta E$ , eV) for the redox changes exhibited by copper and gold complexes.<sup>a</sup>

Complex	Reduction		$E_{\text{LUMO}}$ eV	Oxidation				$E_{\text{HOMO}}$ eV	$\Delta E$ eV
	$E_{\text{M(1)/M(0)}}$	$E_{\text{onset red}}$		$E_{1\text{st}}$	$E_{\text{onset ox}}$	$E_{2\text{nd}}$	$E_{3\text{rd}}$		
$(^{\text{Me}2}\text{L})\text{CuCl}$	-2.70	-2.57	-2.82	+0.53	+0.24	+0.78	–	-5.63	2.81
$(^{\text{Me}2}\text{L})\text{CuBr}$	-2.77	-2.58	-2.81	+0.43	+0.10	+0.67	–	-5.49	2.68
$(^{\text{Me}2}\text{L})\text{CuI}$	-2.58 -2.73	-2.46	-2.93	+0.06	-0.10	+0.28	+0.60	-5.29	2.36
$(^{\text{Me}2}\text{L})\text{CuNCS}$	-2.71	-2.48	-2.91	+0.38	+0.16	+0.68	–	-5.55	2.64
$[(^{\text{Me}2}\text{L})_2\text{Cu}]\text{I}$	-2.47*(65)	-2.39	-3.00	+0.02	-0.11	+0.27	–	-5.28	2.28
$(^{\text{Et}2}\text{L})\text{CuCl}$	-2.82	-2.71	-2.68	+0.57	+0.35	+0.80	–	-5.74	3.21
$(^{\text{Et}2}\text{L})\text{CuBr}$	-2.71	-2.59	-2.80	+0.52	+0.28	+0.72*	–	-5.67	2.87
$[(^{\text{Et}2}\text{L})\text{CuNCS}]_2$	-2.78	-2.53	-2.86	+0.48	+0.19	+0.72*	–	-5.58	2.72
$[(^{\text{Et}2}\text{L})_2\text{Cu}]\text{I}$	-2.50*(70)	-2.43	-2.96	-0.02	-0.15	+0.28	–	-5.24	2.28
$(^{\text{Ad}}\text{L})\text{CuNCS}$	-2.59 -2.71	-2.47	-2.92	+0.67	+0.49	+0.81	–	-5.88	2.96

<sup>a</sup> In MeCN solution, recorded using a glassy carbon electrode, concentration 1.4 mM, supporting electrolyte  $[\text{n-Bu}_4\text{N}][\text{PF}_6]$  (0.13 M), measured at 0.1  $\text{V s}^{-1}$ .

The oxidation of mono(carbene) halides ( $^{\text{R}}\text{L})\text{CuX}$  ( $\text{X} = \text{Cl}, \text{Br}, \text{SCN}$ ) as well as bis(carbene) complexes  $[(^{\text{R}}\text{L})_2\text{Cu}]\text{I}$  exhibits two irreversible oxidation processes at all voltage scan rates. The behavior of the mono(carbene) halides differs from the bis(carbene) complexes which show back-peaks for both irreversible oxidation processes. The copper iodide  $(^{\text{Me}2}\text{L})\text{CuI}$  shows more complex behavior and possesses a third irreversible oxidation process with a back peak at all voltage scan rates (see SI, Figure S21). The onset oxidation potential for copper halide complexes shows well-pronounced cathodic shift in the range of  $\text{Cl} < \text{Br} < \text{I}$  which is in agreement with our previous data on the analogous more bulky  $(^{\text{Ad}}\text{L})\text{CuX}$  compounds.<sup>[1]</sup>

At all scan rates, gold phenolate complexes show quasi-reversible (except **AuO2**) (SI, Figures S27 – S30) and copper phenolates irreversible metal-centred reduction processes (with no back peak) (see SI, Figures S24 – S26) (Table 7). The thiophenolates **AuS1** and **CuS1** exhibit similar behavior, although for **CuS1** the back-peak becomes apparent at scan rates higher than 500 mVs<sup>-1</sup>. The quasi-reversible character is more pronounced for **AuS1** compared to the phenolate analogue **AuO1** (see SI, Figure S29). For instance, the peak-to-peak separation  $\Delta E_p$  is slightly smaller for **AuS1** (76 mV) compared to **AuO1** (80 mV). At the same time the  $i_{pa}/i_{pc}$  ratio for **AuS1** is much closer to unity even at low scan rates (0.66 at 100 mVs<sup>-1</sup> and 0.78 at 1.5 Vs<sup>-1</sup>) compared to **AuO1** (0.48 at 100 mVs<sup>-1</sup> and 0.81 at 1.5 Vs<sup>-1</sup>). The reduction peak is cathodically shifted by 0.2 – 0.3 V for all complexes compared to their chloride analogues, hence they are less easily reduced.

The anilide complexes **CuN1**, **AuN1**, and **AuN4** show a quasi-reversible metal-centered reduction process, while the fluorinated compounds exhibit an irreversible reduction with no back-peak at all scan rates. All anilide complexes show a continuous anodic shift of the equilibrium potential due to reference potential drift, therefore the varied scan rate studies for anilide complexes will not be discussed here.

All phenolate and anilide complexes show two irreversible oxidation waves with no back-peaks at all scan rates. Copper thiophenolate exhibits four irreversible oxidation processes (SI, Figure S26), while for the gold analogue only three waves were observed due to overlapping signals (SI, Figure S29). As expected, the oxidation potential of gold complexes is higher by 0.1 – 0.3 V compared to their copper analogues. The position of the redox potentials is strongly dependent on the nature of the substituents. For instance, phenolate **CuO2**, with electron-withdrawing fluorine substituents, exhibits an anodic shift of 0.27 V of the reduction potential compared to unsubstituted phenolate **CuO1**. At the same time, phenolates **CuO4**, **CuO5**, **AuO3**, and **AuO4**, with electron donating phenyl substituents, show a cathodic shift by *ca.* 0.1 V for the first oxidation potential compared to **CuO1** and **AuO1** and are hence easier to oxidize. For all complexes the first oxidation processes is tentatively assigned to the oxidation of the amide or phenolate ligands, based on the similar electrochemical behavior of various aniline or phenol compounds.<sup>[31]</sup> The estimated HOMO/LUMO energy levels were identified based on first reduction and oxidation potentials;<sup>[32]</sup> these energy values guide the use of these compounds in the fabrication of light emitting devices, which is currently going on in our laboratories.<sup>[33]</sup>

**Table 7.** Formal electrode potentials, onset potentials peak-to-peak separation in parentheses for quasi-reversible process,  $E_{HOMO}/E_{LUMO}$  and band gap values for the redox changes exhibited by copper and gold complexes.<sup>a</sup>

Complex	Reduction		$E_{LUMO}$ eV	Oxidation				$E_{HOMO}$ eV	$\Delta E$ eV
	$E_{M(I)/M(0)}$	$E_{onset\ red}$		$E_{1st}$	$E_{onset\ ox}$	$E_{2nd}$	$E_{3rd}$		
<b>CuO1</b>	-3.03	-2.91	-2.48	+0.28	+0.12	+1.05	–	-5.51	3.03
<b>CuO2</b>	-2.76	-2.65	-2.74	-0.02	-0.13	+1.16	–	-5.26	2.52
<b>CuO4</b>	-2.97	-2.82	-2.57	+0.17	+0.01	+0.80	+0.99	-5.40	2.83
<b>CuO5</b>	-2.93	-2.78	-2.61	+0.19	+0.00	+1.11	–	-5.39	2.78
<b>AuO1</b>	-2.71* (80)	-2.63	-2.82	+0.55	+0.46	+1.30	–	-5.85	3.03
<b>AuO2</b>	-2.69	-2.52	-2.87	+0.01	-0.09	+0.80	–	-5.30	2.43
<b>AuO3</b>	-2.74* (77)	-2.64	-2.75	+0.32	+0.17	+1.01	–	-5.56	2.81
<b>AuO4</b>	-2.66* (85)	-2.58	-2.81	+0.48	+0.32	+1.24	–	-5.71	2.90
( <sup>Ad</sup> L)CuSPh	-2.88	-2.75	-2.64	-0.15	-0.27	+0.34	+0.89 $E_{4th}$ +1.27	-5.12	2.48
( <sup>Ad</sup> L)AuSPh	-2.67* (76)	-2.58	-2.81	+0.37	+0.33	+1.19	+1.31	-5.72	2.91
<b>CuN1</b>	-2.93* (91)	-2.82	-2.57	-0.25	-0.38	+0.61	+0.88	-5.01	2.44
<b>AuN1</b>	-2.95* (65)	-2.86	-2.53	-0.14	-0.24	+0.61	+1.13	-5.15	2.62
<b>CuN2</b>	-3.08	-2.90	-2.49	+0.16	+0.01	+0.83	+1.13	-5.40	2.91
<b>AuN2</b>	-2.86	-2.65	-2.74	+0.37	+0.26	+1.13	–	-5.65	2.91
<b>AuN3</b>	-2.82 -2.71	-2.58	-2.81	+0.38	+0.24	+1.17	–	-5.65	2.82
<b>AuN4</b>	-2.99* (78)	-2.90	-2.49	+0.11	-0.01	+0.90	–	-5.38	2.89

<sup>a</sup> In MeCN solution, recorded using a glassy carbon electrode, concentration 1.4 mM (with exception of 0.7 mM for AuO1) supporting electrolyte [n-Bu<sub>4</sub>N][PF<sub>6</sub>] (0.13 M), measured at 0.1 V s<sup>-1</sup>.

## Conclusion

The reaction of CAAC ligands with copper and gold halides and pseudo-halides gives the corresponding air- and moisture stable adducts. Most of them are simple linear compounds without close metal-metal interactions in the solid state. The optimal synthetic route depends on steric parameters, although the order of addition and the reaction temperature were found to be of primary importance for obtaining either mono- or bis(carbene) complexes selectively. Most of these CAAC complexes are photoluminescent. The luminescence intensity increases with increasing bulkiness of the carbene ligand, in the sequence <sup>Me2</sup>L < <sup>Et2</sup>L < <sup>Ad</sup>L. The emission colors of simple copper halide and pseudo-halide compounds ranged from blue and white to yellow. Gold pseudo-halides were found to be non-emissive.

Crystalline copper chlorides display broad white ( ${}^{\text{Me}2}\text{LCuCl}$ ) to blue-white ( ${}^{\text{Et}2}\text{LCuCl}$ ) fluorescence, with half-widths  $\approx 6300\text{--}6500\text{ cm}^{-1}$ , whereas the bis(carbene) compound [ ${}^{\text{Et}2}\text{L}$ ] ${}_{2}\text{Cu}$ ]I gives a very narrow emission, with a half-width of only  $2200\text{ cm}^{-1}$ . Both the neutral mono(carbene) and ionic bis(carbene) halide complexes of  ${}^{\text{Me}2}\text{L}$  and  ${}^{\text{Et}2}\text{L}$  ligands exhibit prompt fluorescence with lifetimes in the ns range, as well as less intense emissions in the microsecond range. While the latter is present in high-purity samples, its intensity increases with handling and photodegradation due to the photosensitivity of  ${}^{\text{Me}2}\text{L}$  copper complexes.

The emission mechanism depends on the ligand *trans* to the carbene and the type of the charge transfer transition. Fluorescence involving MLCT and  $(\sigma + X)\text{--}\pi^{*}$  transitions was observed for halides, pseudo-halides, and bis(carbene) complexes, whereas copper and gold aryloxides and anilides show LMLCT-type delayed emissions. Within the series of  $({}^{\text{Ad}}\text{L})\text{M}$  aryloxo complexes, electron-withdrawing or *ortho*-substituents reduced the PLQY. As calculations show, the excitation is connected with charge transfer from the phenolate to the carbene ligand. The solid-state photoluminescence intensity is strongly influenced by the M-O-C-C torsion angle, with angles  $>50^{\circ}$  leading to quenching. These observations correlate well with the calculated oscillator strengths for these geometries, which were shown to be a function of the torsion angle. Substitution of halide ligands by phenolates and anilides shifts the reduction potential to higher cathodic values. Copper and gold phenolate and anilide complexes are the most promising candidates for the fabrication of efficient light-emitting devices based on their photophysical behavior and HOMO/LUMO energy levels. Currently, our efforts are focused on testing these materials for use as photoemitters in OLEDs (for neutral compounds) and light-emitting electrochemical cells (LECs, for cationic compounds).<sup>[33]</sup>

### Acknowledgements

This work was supported by the ERC, the Royal Society, and by the Academy of Finland (Project 251448). M. B. is an ERC Advanced Investigator Award holder (grant no. 338944-GOCAT). The computations were made possible by use of the Finnish Grid Infrastructure resources. We thank Dr. R. Blagg, Dr. J. Buttress and Dr. James Courtney for assistance with electrochemical measurements.

### Supporting Information

Supporting information (SI) available: Synthesis and Characterization of Complexes, UV and photoluminescence data, electrochemical data, X-ray crystal structure and refinement data, computational details. CCDC numbers 1522320 - 1522339 contain the supplementary crystallographic data for this paper. These data can be obtained free of charge from The Cambridge Crystallographic Data Centre via

[www.ccdc.cam.ac.uk/data\\_request/cif](http://www.ccdc.cam.ac.uk/data_request/cif). For SI and crystallographic data in CIF or other electronic format see DOI: 10.1039/XXXXXX.

## Footnotes

\* Corresponding authors: [asromanov5@gmail.com](mailto:asromanov5@gmail.com), [mikko.linnolahti@uef.fi](mailto:mikko.linnolahti@uef.fi), [djnc3@cam.ac.uk](mailto:djnc3@cam.ac.uk), [m.bochmann@uea.ac.uk](mailto:m.bochmann@uea.ac.uk)

## References

- [1] A. S. Romanov, D. Di, Le Yang, J. Fernandez-Cestau, C. R. Becker, C. E. James, B. Zhu, M. Linnolahti, D. Credgington, M. Bochmann, *Chem. Commun.* **2016**, 52, 6379.
- [2] R. Visbal, M. C. Gimeno, *Chem. Soc. Rev.* **2014**, 43, 3551–3574.
- [3] K. Matsumoto, N. Matsumoto, A. Ishii, T. Tsukada, M. Hasegawa, T. Tsubomura, *Dalton Trans.* **2009**, 6795-6801.
- [4] (a) V. J. Catalano, A. L. Moore, J. Shearer, J. Kim, *Inorg. Chem.* **2009**, 48, 11362-11375. (b) A. K. Ghosh, V. J. Catalano, *Eur. J. Inorg. Chem.* **2009**, 1832-1843. (c) C. E. Strasser, V. J. Catalano, *J. Am. Chem. Soc.* **2010**, 132, 10009-10011. (d) V. J. Catalano, L. B. Munro, C. E. Strasser, A. F. Samin, *Inorg. Chem.* **2011**, 50, 8465-8476. (e) C. E. Strasser, V. J. Catalano, *Inorg. Chem.* **2011**, 50, 11228-11234. (f) O. Elbjeirami, M. D. Rashdan, V. Nesterov, M. A. Rawashdeh-Omary, *Dalton Trans.* **2010**, 39, 9465-9468.
- [5] Examples of three-coordinate Cu complexes: (a) V. A. Krylova, P. I. Djurovich, M. T. Whited, M. E. Thompson, *Chem. Commun.* **2010**, 46, 6696–6698. (b) M. J. Leidl, V. A. Krylova, P. I. Djurovich, M. E. Thompson, H. Yersin, *J. Am. Chem. Soc.* **2014**, 136, 16032–16038. (c) R. Marion, F. Sguerra, F. DiMeo, E. Sauvageot, J. F. Lohier, R. Daniellou, J. L. Renaud, M. Linares, M. Hamel, S. Gaillard, *Inorg. Chem.* **2014**, 53, 9181-9191.
- [6] (a) H. M. J. Wang, C. Y.L. Chen, I. J. B. Lin, *Organometallics* **1999**, 18, 1216-1223. (b) H. M. J. Wang, C. S. Vasam, T. Y. R. Tsai, S. H. Chen, A. H. H. Chang, I. J. B. Lin, *Organometallics* **2005**, 24, 486-493.
- [7] A. Gómez-Suárez, D. J. Nelson, D. G. Thompson, D. B. Cordes, D. Graham, A. M. Z. Slawin, S. P. Nolan, *Beilstein J. Org. Chem.* **2013**, 9, 2216-2223.
- [8] R. Visbal, I. Ospino, J. M. López-de-Luzuriaga, A. Laguna, M. C. Gimeno, *J. Am. Chem. Soc.* **2013**, 135, 4712-4715.
- [9] O. Back, M. Henry-Ellinger, C. D. Martin, D. Martin, G. Bertrand, *Angew. Chem. Int. Ed.* **2013**, 52, 2939 –2943.

- [10] Guido D. Frey, Rian D. Dewhurst, Shazia Kousar, Bruno Donnadiu, Guy Bertrand, *J. Organomet. Chem.* **2008**, *693*, 1674–1682.
- [11] A. S. Romanov, M. Bochmann, *Organometallics* **2015**, *34*, 2439–2454.
- [12] (a) H. Braunschweig, W. C. Ewing, T. Kramer, J. D. Mattock, A. Vargas, C. Werner, *Chem. Eur. J.* **2015**, *21*, 12347 – 12356. (b) X. Hu, M. Soleilhavoup, M. Melaimi, J. Chu, G. Bertrand, *Angew. Chem. Int. Ed.* **2015**, *54*, 608–6011.
- [13] M. Gernert, U. Müller, M. Haehnel, J. Pflaum, A. Steffen, *Chem. Eur. J.*, accepted manuscript, DOI 10.1002/chem.201605412.
- [14] (a) J. A. Kargol, R. W. Creceley, J. L. Burmeister, *Inorg. Chem.* **1979**, *18*, 2532–2535; (b) C.A. Dodds, A.R. Kennedy, *Z. Anorg. Allg. Chem.* **2014**, *640*, 926–930.
- [15] R. A. Bailey, S. L. Kozak, T. W. Michelsen, W. N. Mills, *Coord. Chem. Rev.* **1971**, *6*, 407–445.
- [16] T. Mathieson, A. Schier, H. Schmidbaur, *J. Chem. Soc., Dalton Trans.* **2001**, 1196–1200.
- [17] M. V. Baker, P. J. Barnard, S. K. Brayshaw, J. L. Hickey, B. W. Skelton, A.H. White, *Dalton Trans.* **2005**, 37–43.
- [18] The synthesis of (<sup>E</sup>L)CuOPh via a two-step procedure using (<sup>E</sup>L)CuO<sup>t</sup>Bu has recently been reported: L. Jin, E. A. Romero, M. Melaimi, G. Bertrand, *J. Am. Chem. Soc.*, **2015**, *137*, 15696–15698.
- [19] (a) S. A. Delp, C. Munro-Leighton, L. A. Goj, M. A. Ramírez, T. B. Gunnoe, J. L. Petersen, P. D. Boyle, *Inorg. Chem.* **2007**, *46*, 2365–2367; (b) F. Cisnetti, P. Lemoine, M. El-Ghozzi, D. Avignant, A. Gautier, *Tetrahedr. Lett.*, **2010**, *51*, 5226–5229.
- [20] (a) H. Schmidbaur, A. Schier, *Chem. Soc. Rev.* **2008**, *37*, 1931–1951. (b) H. Schmidbaur, A. Schier, *Chem. Soc. Rev.* **2012**, *41*, 370–412.
- [21] A. Bondi, *J. Phys. Chem.* **1964**, *68*, 441–451.
- [22] K. A. Vinogradova, V. F. Plyusnin, A. S. Kupryakov, M. I. Rakhmanova, N. V. Pervukhina, D. Y. Naumov, L. A. Sheludyakova, E. B. Nikolaenkova, V. P. Krivopalov, M. B. Bushuev, *Dalton Trans.* **2014**, *43*, 2953–2960.
- [23] P. C. Ford, E. Cariati, J. Bourassa, *Chem. Rev.* **1999**, *99*, 3625–3647.
- [24] (a) M. Osawa, *Chem. Commun.* **2014**, *50*, 1801–1803. (b) T. Hofbeck, U. Monkowius, H. Yersin, *J. Am. Chem. Soc.* **2015**, *137*, 399–404.
- [25] Recent examples of four-coordinate Cu halides: (a) A. Tsuboyama, K. Kuge, M. Furugori, S. Okada, M. Hoshino, K. Ueno, *Inorg. Chem.* **2007**, *46*, 1992–2001. (b) A. Kobayashi, K. Komatsu, H. Ohara, W. Kamada, Y. Chishina, K. Tsuge, H. C. Chang, M. Kato, *Inorg. Chem.* **2013**, *52*, 1388–1398. (c) M. J. Leitl, F.-R. Küchle, H. A. Mayer, L. Wesemann, H. Yersin, *J. Phys. Chem. A* **2013**, *117*, 11823–11836. (d) D. M. Zink, D. Volz, T. Baumann, M. Mydlak, H. Flügge, J.

- Friedrichs, M. Nieger, S. Bräse, *Chem. Mater.* **2013**, *25*, 4471–4486. (e) D. M. Zink, M. Bachle, T. Baumann, M. Nieger, M. Kuhn, C. Wang, W. Klopfer, U. Monkowius, T. Hofbeck, H. Yersin, S. Bräse, *Inorg. Chem.* **2013**, *52*, 2292–2305. (f) M. W. Hong, L. Song, Y. Zhao, L. S. Qin, C. Y. Wang, H. S. Shi, J. Y. Guo, X. D. Tao, K. Y. Shu, W. X. Chai, *J. Cluster Sci.* **2014**, *25*, 1627–1640. (g) H. Ohara, A. Kobayashi, M. Kato, *Dalton Trans.* **2014**, *43*, 17317–17323. (h) M. Wallesch, D. Volz, D. M. Zink, U. Schepers, M. Nieger, T. Baumann, S. Bräse, *Chem. Eur. J.* **2014**, *20*, 6578–6590. (i) T. Gneuß, M. J. Leitzl, L. H. Finger, N. Rau, H. Yersin, J. Sundermeyer, *Dalton Trans.* **2015**, *44*, 8506–8520. (j) K. Chen, J. Shearer, V. J. Catalano, *Inorg. Chem.* **2015**, *54*, 6245–6256. (k) D. Volz, Y. Chen, M. Wallesch, R. Liu, C. Fléchon, D. M. Zink, J. Friedrichs, H. Flügge, R. Steininger, J. Göttlicher, C. Heske, L. Weinhardt, S. Bräse, F. So, T. Baumann, *Adv. Mater.* **2015**, *27*, 2538–2543. (l) D. Volz, M. Wallesch, S. L. Grage, J. Göttlicher, R. Steininger, D. Batchelor, T. Vitova, A. S. Ulrich, C. Heske, L. Weinhardt, T. Baumann, S. Bräse, *Inorg. Chem.* **2014**, *53*, 7837–7847.
- [26] Halide-free Cu complexes: (a) D. Felder, J.-F. Nierengarten, F. Barigelletti, B. Ventura, N. Armaroli, *J. Am. Chem. Soc.* **2001**, *123*, 6291–6299. (b) A. J. M. Miller, J. L. Dempsey, J. C. Peters, *Inorg. Chem.* **2007**, *46*, 7244–7246. (c) J. C. Deaton, S. C. Switalski, D. Y. Kondakov, R. H. Young, T. D. Pawlik, D. J. Giesen, S. B. Harkins, A. J. M. Miller, S. F. Mickenberg, J. C. Peters, *J. Am. Chem. Soc.* **2010**, *132*, 9499–9508. (d) R. Czerwieniec, J. Yu, H. Yersin, *Inorg. Chem.* **2011**, *50*, 8293–8301. (e) A. Kaeser, M. Mohankumar, J. Mohanraj, F. Monti, M. Holler, J.-J. Cid, O. Moudam, I. Nierengarten, L. Karmazin-Brelot, C. Duhayon, B. Delavaux-Nicot, N. Armaroli, J.-F. Nierengarten, *Inorg. Chem.* **2013**, *52*, 12140–12151. (f) R. Czerwieniec, K. Kowalski, H. Yersin, *Dalton Trans.* **2013**, *42*, 9826–9830. (g) X.-L. Chen, R. Yu, Q.-K. Zhang, L.-J. Zhou, X.-Y. Wu, Q. Zhang, C.-Z. Lu, *Chem. Mater.* **2013**, *25*, 3910–3920. (h) C. L. Linfoot, M. J. Leitzl, P. Richardson, A. F. Rausch, O. Chepelin, F. J. White, H. Yersin, N. Robertson, *Inorg. Chem.* **2014**, *53*, 10854–10861. (i) C. Bizzarri, C. Strabler, J. Prock, B. Trettenbrein, M. Ruggenthaler, C.-H. Yang, F. Polo, A. Iordache, P. Brügge, L. De Cola, *Inorg. Chem.* **2014**, *53*, 10944–10951.
- [27] H. Yersin, A. F. Rausch, R. Czerwieniec, T. Hofbeck, T. Fischer, *Coord. Chem. Rev.* **2011**, *255*, 2622–2652.
- [28] (a) M. Osawa, M. Hoshino, M. Hashimoto, I. Kawata, S. Igawa, M. Yashima, *Dalton Trans.*, **2015**, *44*, 8369; (b) M. Hashimoto, M. Igawa, M. Yashima, I. Kawata, M. Hoshino, M. Osawa, *J. Am. Chem. Soc.*, **2011**, *133*, 10348.
- [29] The observed long-lived emission corresponds to the recent report by Gernert et al. on phosphorescence behavior [13]. However, all sublimed samples of (<sup>Me2</sup>L)CuCl show emission at

483 nm. We were unable to confirm their reported emission maxima of 511 and 512 nm for  $(^{\text{Me}2}\text{L})\text{CuCl}$  and  $(^{\text{Me}2}\text{L})\text{CuBr}$ , respectively.

- [30] By comparison, transient absorption kinetics of  $(^{\text{Ad}}\text{L})\text{CuCl}^{[1]}$  indicate a single photoexcited species, 70% of which is lost within 1 ns (SI, Figure S12).
- [31] (a) F. Fabrizi de Biani, M. Corsini, P. Zanello, *Redox Chemistry and Electrochemistry of Homoleptic Metal Phenolates*. PATAI's Chemistry of Functional Groups, Wiley 2013. DOI: 10.1002/9780470682531.pat0600. (b) K. Karon, M. Lapkowski, *J. Solid State Electrochem.* **2015**, *19*, 2601-2610. (c) G. A. Sotzing, J. L. Reddinger, A. R. Katritzky, J. Soloducho, R. Musgrave, J. R. Reynolds, *Chem. Mater.* **1997**, *9*, 1578-1587. (d) H. Yang, A. J. Bard, *J. Electroanal. Chem.*, **1991**, *306*, 87-109.
- [32] C. M. Cardona, W. Li, A. E. Kaifer, D. Stockdale, G. C. Bazan, *Adv. Mater.*, **2011**, *23*, 2367-2371.
- [33] Preprint: D. Di, A. S. Romanov, L. Yang, S. T. E. Jones, R. H. Friend, M. Linnolahti, M. Bochmann, D. Credginton, *Highly efficient light-emitting diodes based on intramolecular rotation*, Cornell University Library, 2016, <https://arxiv.org/abs/1606.08868>.